A molecularly defined basalo-prefrontal-thalamic circuit regulates sensory and affective dimensions of pain

Guoguang Xie[1,2,3], Yiqiong Liu[1,2,3], Xuetao Qi[1,2,3], Aritra Bhattacherjee[1,2,3], Chao Zhang[1,2,3], and Yi Zhang[1,2,3,4,5*]

[1]Howard Hughes Medical Institute, Boston Children's Hospital, Boston, Massachusetts 02115, USA; [2]Program in Cellular and Molecular Medicine, Boston Children's Hospital, Boston, Massachusetts 02115, USA; [3]Division of Hematology/Oncology, Department of Pediatrics, Boston Children's Hospital, Boston, Massachusetts 02115, USA; [4]Department of Genetics, Harvard Medical School, Boston, Massachusetts 02115, USA; [5]Harvard Stem Cell Institute, WAB-149G, 200 Longwood Avenue, Boston, Massachusetts 02115, USA.

[*]To whom correspondence should be addressed
E-mail: yzhang@genetics.med.harvard.edu

Keywords: Pain, mPFC, thalamus, *Foxp2*-expressing neuron

Manuscript information: 49 pages, 8 Figures, 7 Extended Data Figures

Abstract

Both the medial prefrontal cortex (mPFC) and thalamus have been implicated in pain regulation. However, the roles of the mPFC-thalamus connection in pain and how the mPFC modulates nociceptive processing within the brain remain unclear. Here, we show that the mPFC neurons that project to thalamus are marked by *Foxp2* expression and deactivated in both acute and chronic pain. Persistent inactivation of the mPFC *Foxp2*$^{+}$ neurons enhances nociceptive sensitivity, while their activation alleviates multiple aspects of pain. Circuit-specific manipulations revealed that the projections to parataenial nucleus, mediodorsal and ventromedial thalamus differentially modulate sensory and affective pain. Additionally, the mPFC *Foxp2*$^{+}$ neurons receive cholinergic input from the basal forebrain, particularly the horizonal diagonal band (HDB). Notably, activation of the α4β2-containing nicotinic acetylcholine receptor in mPFC exerts antinociceptive effects in *Foxp2*$^{+}$ neuron-dependent manner. Together, our study defines an HDB→mPFC^{Foxp2}→thalamus circuit essential for sensory and affective pain modulation and underscores the therapeutic potential of targeting mPFC cholinergic signaling in chronic pain management.

Introduction

Pain is an unpleasant sensory and emotional experience associated with actual or potential tissue damage and is essential to protect the body from potentially harmful stimuli[1, 2]. Chronic pain, however, is not just a temporal continuum of acute pain but one of the major causes of human suffering, affecting about 20% of the global population with immense clinical and economic consequences[3, 4]. Unfortunately, current pain management strategies are largely unsatisfactory with inadequate pain relief and multiple adverse effects[5, 6]. Thus, understanding the mechanisms underlying pain processing remains to be an urgent need for developing effective treatments.

Accumulating evidence supports the crucial roles of medial prefrontal cortex (mPFC) in regulating multiple aspects of pain, including the sensory, affective and cognitive dimensions[7-11]. Neuroimaging studies in humans have showed functional deactivation and altered connectivity of mPFC in patients with chronic pain[12-14]. Consistently, preclinical studies have also revealed the diminished activities of mPFC in several forms of chronic pain and the critical roles of mPFC in pain relief[15-18]. The mPFC is widely connected with other brain regions, including the periaqueductal gray (PAG), thalamus, amygdala and basal nuclei[19]. As part of the descending modulation pathway that governs the noxious inputs in the spinal cord, the mPFC to PAG circuit in pain processing has been well documented[5, 16, 17]. However, it is much less clear about the roles of the mPFC outputs to other brain regions in pain regulation as well as how mPFC modulates the processing of noxious information in the brain.

Thalamus, a major target of the mPFC output, serves as a key hub for integrating and processing nociceptive information ascending from the spinal cord and modulates both sensory and affective dimensions of pain through the lateral and medial pathways[5, 20]. Imaging studies have linked chronic pain to thalamic alterations, including reduced volume, activity and imbalanced transmitters[12, 14, 21]. Recent findings also highlight the critical functions of the connections between

thalamus and other cortices, such as motor cortex and ACC, in regulating affective pain[22, 23]. Despite the strong anatomical connections between mPFC and thalamus and their critical roles in pain and other behaviors such as attention and cognition[24, 25], the specific functions of the mPFC to thalamus circuit in pain processing remain largely unexplored.

The mPFC receives inputs from multiple brain regions[19]. Among these, the strengthened glutamatergic input from basolateral amygdala (BLA), which synapses onto the inhibitory neurons in mPFC and sends feedforward inhibition to the pyramidal neurons, has been reported as a key mechanism underlying the deactivation of mPFC in chronic pain.[17, 18]. However, the roles of other mPFC inputs in chronic pain remain largely unknown. Notably, the mPFC receives dense cholinergic innervation from the basal forebrain, a pathway involved in various functions such as learning, attention and arousal[26]. Although the clinical importance of cholinergic signaling in pain has been well recognized[27], the roles and the circuit mechanism of cholinergic modulation of mPFC in pain are not fully understood. Moreover, the mPFC is highly heterogeneous, with differential structural and functional dysregulation of mPFC in chronic pain[8]. The variable functional responses, either pain relief or exacerbation following mPFC activation[8, 28, 29], might result from the cell heterogeneity across subregions and layers of mPFC, which requires higher cell-type and projection-specific resolution to accurately delineate.

In this study, we identify *Foxp2* as a marker of the mPFC neurons that project to the thalamus and show that these neurons are deactivated under acute and chronic pain. Using cell type-specific and circuit-specific manipulations, we demonstrate that activation of the mPFC *Foxp2*$^+$ neurons alleviates both the sensory and affective components of pain by targeting distinct thalamic subregions. Additionally, we show that the mPFC *Foxp2*$^+$ neurons receive cholinergic innervation from the basal forebrain, particularly the horizonal diagonal band of Broca (HDB), and that activation of the cholinergic projection is antinociceptive. Notably, we found that activation of the α4β2-containing nicotinic acetylcholine receptor (nAChR) in mPFC relieves pain, which requires

the *Foxp2*$^{+}$ neuronal activity. Collectively, our study reveals a novel mechanism by which the mPFC regulates pain through projection to thalamus, and highlights mPFC cholinergic signaling as a potential therapeutic target for chronic pain treatment.

Results

Foxp2 specifically marks the mPFC outputs to thalamus

The cerebral cortex is organized into layers with diverse neuron subtypes that have distinct projection patterns distributed in laminar pattern[30]. In the mPFC, the projections to thalamus, a hub for pain processing, primarily originate from the layer (L) 6 corticothalamic (CT) neurons[31, 32]. Surprisingly, single molecule fluorescence *in situ* hybridization (smFISH) revealed that *Ntsr1*, a widely used L6 CT neuron marker in the cortex[22, 33, 34], is broadly expressed from L2 to L6 in the mPFC (Extended Data Fig. 1a), indicating the different organization of the mPFC compared to other cortex. Integrative analysis of our previous single-cell RNA sequencing and spatial transcriptomic data indicated *Foxp2* and *Oprk1* respectively mark the L6 CT and L6 intratelencephalic (IT) neurons[35, 36], the two major excitatory neuron types in L6 (Extended Data Fig. 1b). This is consistent with previous studies suggesting exclusive expression of *Foxp2* in CT neurons of the sensory cortex[33, 37-40].

To determine whether *Foxp2* can serve as a marker for L6 CT neurons in the mPFC of adult mice, we injected cholera toxin subunit B (CTB) 555, a retrograde tracer, into the medial dorsal thalamus (MD) and performed smFISH for *Foxp2* in the mPFC (Fig. 1a). We found that the CTB$^+$ cells are mainly located in L6 with over 90% of them express *Foxp2* (Fig. 1a), indicating that the *Foxp2*$^+$ neurons account for the major outputs of mPFC to thalamus. Around 60% of the *Foxp2*$^+$ neurons are labeled by CTB, which could be due to the limited area of CTB diffusion and that the mPFC *Foxp2*$^+$ neurons may project to other thalamic regions. To examine whether the mPFC *Foxp2*$^+$ neurons project to other major mPFC targets, CTB was also injected into the PAG (Fig. 1b), contralateral mPFC (Extended Data Fig. 1c), amygdala (Extended Data Fig. 1d) or nucleus accumbens (NAc) (Extended Data Fig. 1e). Minimal colocalization of CTB and *Foxp2* was observed in these conditions (Fig. 1b and Extended Data Fig. 1c-e). These findings confirm that *Foxp2* specifically marks the major outputs of mPFC to thalamus.

126

127 Given the outputs of mPFC to thalamus mainly originate from the L6 CT neurons, we then asked
128 whether *Foxp2* specifically marks this distinct neuronal subtype. To this end, we performed
129 smFISH for *Foxp2*, *Slc17a7* (a marker for glutamatergic neurons) and *Gad1* (a marker for
130 inhibitory neurons), which revealed that over 95% of *Foxp2*$^+$ cells express *Slc17a7* (Fig. 1c),
131 indicating that *Foxp2*$^+$ cells are predominantly glutamatergic neurons. To further characterize the
132 distribution of *Foxp2*$^+$ cells in the mPFC, smFISH for *Foxp2, Etv1* (a marker for L5), and *Ctgf* (a
133 marker for L6b) was performed with the mPFC sections along the anterior-posterior axis (Fig. 1d
134 and Extended Data Fig. 2). Quantification of the fluorescence signals confirmed the expression of
135 *Foxp2* in L6 including L6b, with about 10% of *Foxp2*$^+$ cells also expressing *Etv1* (Fig. 1d and
136 Extended Data Fig. 2a-c). Further quantification of the fluorescence signals in the mPFC from pia
137 to white matter revealed that the *Foxp2*$^+$ cells are mainly located in L6 and to a much less extent
138 in deep L5, especially in the anterior part of mPFC (Extended Data Fig. 2d). Since *Foxp2* and
139 *Oprk1* are indicated to respectively mark the L6 CT and IT neurons (Extended Data Fig. 1b), we
140 examined their expression in the mPFC and found that they label two distinct neuronal populations
141 in L6 with minimal overlap (Fig. 1e). Because there are also a small number of *Foxp2*$^+$ neurons in
142 L5, where resides the L5 IT neurons, as well as the extratelencephalic (ET) neurons labeled by
143 *Pou3f1*[35] and near-projecting (NP) neurons labeled by *Tshz2*[41], we then performed smFISH and
144 found little overlap between *Foxp2* and *Pou3f1* (Fig. 1f) or *Tshz2* (Fig. 1g). Collectively, these
145 results indicate that *Foxp2* labels a distinct neuronal subtype in L6 different from the IT, ET and
146 NP neurons in the mPFC, consistent with the tracing results.

147

148 To further confirm that the mPFC *Foxp2*$^+$ neurons specifically project to the thalamus, Cre
149 recombinase (Cre)-dependent adeno-associated virus (AAV) encoding mGFP and synaptophysin-
150 fused mRuby that labels axon terminals was injected into the mPFC of *Foxp2*-Cre mice (Fig. 1h).
151 The virus expression was confirmed by *post hoc* histological examination (Extended Data Fig. 1f).
152 Consistent with the fact that *Foxp2* labels the L6 CT neurons in the mPFC, whole brain mapping

153 revealed that the mPFC *Foxp2*$^{+}$ neurons primarily project to thalamus, with the highest intensity
154 of mRuby signals in parataenial thalamic nucleus (PTN), mediodorsal (MD) and ventromedial
155 (VM) thalamus (Fig. 1h). Weaker signals were observed in the nucleus reuniens (Re),
156 paraventricular nucleus of thalamus (PVT) and the medial striatum (Str), while no signal was
157 detected in other downstream targets of mPFC such as NAc, amygdala, PAG, hippocampus,
158 hypothalamus and ventral tegmental area (VTA) (Fig. 1h and Extended Data Fig. 1g-m).
159 Quantification of the average axon-labeling mRuby signals indicated that the medial thalamic
160 nuclei, including PTN, MD and VM, are the main downstream targets of the mPFC *Foxp2*$^{+}$
161 neurons (Fig. 1i). Collectively, these results demonstrate that *Foxp2* specifically labels the mPFC
162 outputs to thalamus (Fig. 1j).
163

164 **The mPFC *Foxp2*$^{+}$ neurons are deactivated in acute and chronic pain**

165 To determine whether the mPFC *Foxp2*$^{+}$ neurons are involved in pain processing, *in vivo*
166 miniscopic calcium (Ca^{2+}) imaging was performed to monitor the activity of the individual mPFC
167 *Foxp2*$^{+}$ neurons under various pain states. To this end, Cre-dependent AAV encoding the Ca^{2+}
168 indicator GCaMP7s was injected into the prelimbic cortex (PL), a subregion of mPFC critical for
169 pain regulation[8], of *Foxp2*-Cre mice, followed by the implantation of a gradient refractive index
170 (GRIN) lens above the injection site two weeks later (Fig. 2a). Virus expression and proper GRIN
171 lens implantation were confirmed by *post hoc* histological examination (Fig. 2a). Four weeks after
172 the virus injection, fluorescence signals of the individual *Foxp2*$^{+}$ neurons were recorded through
173 the GRIN lens using a head-mounted miniaturized microscope, and the Ca^{2+} signal traces of
174 individual neurons were identified and extracted (Fig. 2b). The mice were subjected to acute
175 noxious stimuli and complete Freund's adjuvant (CFA) treatment to induce chronic inflammatory
176 pain, with the Ca^{2+} signals recorded at the indicated time points (Fig. 2c).
177

178 To examine the activities of the *Foxp2*$^{+}$ neurons in response to noxious mechanical stimulation,
179 we recorded the baseline activity for 2 minutes, then subjected the mice to tail pinch for 1 minute,

and monitored an additional 9 minutes for recovery (Fig. 2d). We found that most of the *Foxp2*$^{+}$ neurons exhibited a decreased frequency of Ca^{2+} events during pinch stimulation, followed by a gradual recovery (Fig. 2e). A small subset of the *Foxp2*$^{+}$ neurons displayed the opposite response (Fig. 2e). Quantitative analysis revealed that around 80% of the *Foxp2*$^{+}$ neurons exhibited a significant decrease in the Ca^{2+} event frequency during pinch stimulation compared to the baseline (Fig. 2f and Extended Data Fig. 3a). A significant decrease in the overall Ca^{2+} event frequency across all *Foxp2*$^{+}$ neurons was also observed (Fig. 2g), while the amplitude was unaltered (Extended Data Fig. 3b). These results indicate that the overall *Foxp2*$^{+}$ neuronal activity is decreased in response to noxious mechanical stimulation.

The mice were also subjected to formalin treatment (Fig. 2h), which induces biphasic pain responses as previously described[42]. Enhanced coping behaviors were observed during the first 5 minutes (phase 1) and between 15 to 30 minutes (phase 2) following the formalin injection (Extended Data Fig. 3c). Similar to the responses to noxious mechanical stimulation, a large subset of the *Foxp2*$^{+}$ neurons exhibited a decrease in the frequency of Ca^{2+} events during phase 1, while a small subset showed increased activity (Fig. 2i). Quantitative analysis revealed a significant decrease in the Ca^{2+} event frequency during both phases, with approximately 30% of *Foxp2*$^{+}$ neurons significantly deactivated in the phase 1 (Fig. 2j and Extended Data Fig. 3d). The overall Ca^{2+} event frequency but not amplitude across all *Foxp2*$^{+}$ neurons was also significantly decreased in both phases (Fig. 2k and Extended Data Fig. 3e), indicating a decreased *Foxp2*$^{+}$ neuronal activity in response to formalin treatment. Collectively, these results indicate that the mPFC *Foxp2*$^{+}$ neurons are deactivated in acute nociception.

Finally, we asked whether the mPFC *Foxp2*$^{+}$ neurons are involved in chronic pain. To this end, we subjected the mice to CFA treatment to induce chronic inflammatory pain (Fig. 2l). The overall frequency of Ca^{2+} events in the recorded mPFC *Foxp2*$^{+}$ neurons significantly decreased in both day 1 and day 7 after the CFA injection compared to the baseline (Fig. 2m), indicating a decrease

in the *Foxp2*$^+$ neuronal activity in chronic inflammatory pain. To better compare the Ca^{2+} events of the individual *Foxp2*$^+$ neurons among different days, we identified and analyzed the same neurons recorded in different days (Extended Data Fig. 3f). We found that a large proportion of the *Foxp2*$^+$ neurons exhibited decreased Ca^{2+} activities on day 1 and day 7 after CFA injection (Fig. 2n, o). Quantitative analysis revealed the decreased Ca^{2+} events frequency of the registered *Foxp2*$^+$ neurons in both day 1 and day 7 (Fig. 2p), and that 25.8% and 43.5% of *Foxp2*$^+$ neurons were significantly deactivated on day 1 and day 7, respectively (Fig. 2q, r). Together, these results demonstrate that the mPFC *Foxp2*$^+$ neurons are deactivated in CFA-induced chronic inflammatory pain.

Persistent inactivation of the mPFC *Foxp2*$^+$ neurons enhances nociceptive sensitivity, while activation of these neurons alleviates different aspects of pain

Given the critical roles of mPFC and thalamus in pain processing and the observed deactivation of the mPFC *Foxp2*$^+$ neurons in both acute and chronic pain (Fig. 2), we asked whether these neurons play a causal role in pain regulation. To this end, Cre-dependent AAVs expressing EYFP or tetanus neurotoxin (TeNT) were bilaterally injected into the PL mPFC of *Foxp2*-Cre mice to persistently block the synaptic output of the *Foxp2*$^+$ neurons (Fig. 3a). Behavioral tests were conducted five weeks later, with virus expression confirmed by *post hoc* histological examination (Fig. 3a). We first performed von Frey test (VFT) to measure the mechanical sensitivity of the mice. The TeNT group exhibited a significantly decreased paw withdrawal threshold compared to the control group, indicating that persistent inactivation of the mPFC *Foxp2*$^+$ neurons induces mechanical hypersensitivity of the mice (Fig. 3b). Similarly, a significant decrease in paw withdrawal latency in the hot plate test (HPT) was also observed in the TeNT group, indicating thermal hypersensitivity in these mice (Fig. 3c). Together, these results indicate that persistent inactivation of the mPFC *Foxp2*$^+$ neurons enhances nociceptive sensitivity in mice.

We next asked whether short term manipulation of the mPFC *Foxp2*$^+$ neurons affects the

nociception. To this end, we bilaterally injected Cre-dependent AAVs encoding mCherry or hM3Dq, an activating DREADD (designer receptors exclusively activated by designer drug), into the PL mPFC of the *Foxp2*-Cre mice (Fig. 3d). Virus expression was confirmed by *post hoc* histological examination (Fig. 3d). Three weeks later, behavioral assays were performed 20 min after intraperitoneal (i.p.) injection of clozapine-N-oxide (CNO). In both the VFT and HPT, the hM3Dq group showed a significant increase in paw withdrawal threshold and latency (Fig. 3e), indicating the antinociceptive effects induced by the mPFC *Foxp2*$^+$ neuron activation. To examine the roles of the mPFC *Foxp2*$^+$ neurons in coping behaviors, formalin test was performed which revealed a significant decrease in licking duration in both phase 1 and phase 2 in the hM3Dq group (Fig. 3f), further supporting the antinociceptive effects of the mPFC *Foxp2*$^+$ neuron activation.

We next assessed the roles of the mPFC *Foxp2*$^+$ neurons in chronic pain by treating the mice with CFA to induce chronic inflammatory pain. VFT and HPT were performed 2 or 3 days after CFA injection which revealed significant increases in paw withdrawal threshold and latency in the hM3Dq group (Fig. 3g), indicating activation of the mPFC *Foxp2*$^+$ neurons alleviates the mechanical and thermal hypersensitivity in chronic inflammatory pain. To determine the contribution of these neurons to the affective components of pain, we subjected the mice to a conditioned place preference (CPP) test. The mice were conditioned with saline in one chamber and CNO in another (Fig. 3h). After three days of training, the hM3Dq group displayed a preference for the chamber paired with CNO treatment, as indicated by increased time spent in the chamber and a higher CPP score (Fig. 3h), suggesting that activation of the mPFC *Foxp2*$^+$ neurons could alleviate affective aspects of chronic inflammatory pain. Collectively, these results indicate that activation of the mPFC *Foxp2*$^+$ neurons relieves both nociceptive hypersensitivity and negative affects of chronic inflammatory pain.

To evaluate the effects of short-term inactivation, we bilaterally injected Cre-dependent AAVs expressing mCherry or hM4Di, an inhibitory DREADD, into the PL mPFC of the *Foxp2*-Cre mice

(Extended Data Fig. 4a). Surprisingly, no significant effects were observed in the nociceptive sensitivity, coping behaviors or negative affects of pain as indicated by VFT, HPT, formalin test and CPP test (Extended Data Fig. 4b-d). The efficiency of chemogenetic manipulation was confirmed as the expression of an immediate-early gene cFos was respectively decreased or increased after CNO treatment in the hM4Di or hM3Dq group (Extended Data Fig. 4e).

Collectively, these results indicate that persistent inactivation of the mPFC *Foxp2*$^+$ neurons enhances nociceptive sensitivity, while activation of these neurons exerts robust antinociceptive effects, alleviating both the sensory and affective components of inflammatory pain.

Projection-specific roles of the mPFC *Foxp2*$^+$ neurons in regulating acute and chronic pain

Having demonstrated the crucial roles of the mPFC *Foxp2*$^+$ neurons in regulating pain, we next investigated the underlying circuit mechanisms. We have revealed that the PTN, MD and VM thalamic subregions are the major downstream targets of the mPFC *Foxp2*$^+$ neurons (Fig. 1h, i and Extended Data Fig. 1f-m). Previous studies have revealed the roles of MD and VM in regulating affective, but not sensory aspects of pain[7, 22, 23], while the PTN is much less studied but implicated in regulating pain sensitivity in mice[43]. To determine the roles of the mPFC *Foxp2*$^+$ projections in regulating pain, Cre-dependent AAVs encoding EYFP or channelrhodopsin-2 (ChR2) were injected into the PL mPFC of *Foxp2*-Cre mice, and optical fibers were implanted above the PTN (Fig. 4a), MD (Fig. 4b) or VM (Fig. 4c), respectively for projection-specific activation. Virus expression and fiber implantation were confirmed by *post hoc* histological examination (Fig. 4a-c). Three weeks later, VFT and HPT were conducted. We found that optogenetic activation of the mPFC *Foxp2*$^+$ projection to PTN significantly increased the paw withdrawal threshold in VFT and latency in HPT compared to the baseline or the control group (Fig. 4d), indicating reduced mechanical and thermal sensitivity. In contrast, activation of the projections to MD or VM had no significant effect on nociceptive sensitivity (Fig. 4e, f). These results suggest that mPFC *Foxp2*$^+$ neurons reduce mechanical and thermal sensitivity through projecting to PTN, but not the MD or

VM of thalamus.

To examine the roles of the projections in coping behaviors under tonic pain, we subjected the mice to formalin test with optogenetic activation of the specific projections. We found that activation of the projections to PTN and VM, but not MD, significantly reduced the licking duration in both phase 1 and phase 2 of the formalin test compared to the control group (Fig. 4g-i). These results indicate that the projections of the mPFC *Foxp2*$^{+}$ neurons to the PTN and VM reduce the coping behaviors of the mice in response to tonic pain. Collectively, these results demonstrate that the mPFC^{Foxp2}→PTN circuit modulates both the nociceptive sensitivity and coping behavior and the mPFC^{Foxp2}→VM circuit specifically modulate the coping behavior, while the mPFC^{Foxp2}→MD circuit is not involved in either.

To assess the roles of the projections in chronic pain, we treated the mice with CFA to induce chronic inflammatory pain and performed the pain-related behavioral assays with optogenetic stimulation (Fig. 5a). Two and three days after the CFA injection, VFT and HPT were performed, respectively, to measure mechanical allodynia and thermal hyperalgesia in chronic inflammatory pain. We found that activation of the PTN projection significantly increased the paw withdrawal threshold and latency (Fig. 5b), indicating reduced mechanical and thermal hypersensitivity of the mice. In contrast, no significant change in the VFT and HPT was observed by activating the MD or VM projections (Fig. 5c, d). These results demonstrate that the PTN projection is primarily responsible for the roles of the mPFC *Foxp2*$^{+}$ neurons in alleviating nociceptive hypersensitivity in chronic pain.

To investigate the roles of the projections in regulating affective aspects of chronic pain, we subjected the mice to the CPP test, pairing one chamber with optogenetic stimulation (Fig. 5a). The mice with activation of the PTN or MD projections exhibited a significant increase in the time spent in the light-paired chamber as well as a higher CPP score (Fig. 5e, f), indicating the alleviated

negative affects of pain in these mice. Activation of the VM projection, however, had no significant effects on the chamber preference (Fig. 5g). These results indicate that both the mPFC^{Foxp2}→PTN and mPFC^{Foxp2}→MD circuits alleviate the affective aspects of chronic inflammatory pain, while the mPFC^{Foxp2}→VM circuit is not involved.

Collectively, these results demonstrate that while the mPFC^{Foxp2}→PTN circuit is involved in regulating nociceptive sensitivity, coping behaviors and negative affects of pain, the mPFC^{Foxp2}→MD circuit modulates the negative pain affects and the mPFC^{Foxp2}→VM circuit regulates coping behaviors, respectively.

The mPFC *Foxp2*$^{+}$ neurons receive antinociceptive cholinergic inputs from HDB

Having demonstrated the functional deactivation of the mPFC *Foxp2*$^{+}$ neurons in pain and their pain-relieving effects through projections to distinct thalamic nuclei, we next explored the circuit mechanism regulating the activity of the mPFC *Foxp2*$^{+}$ neurons. Previous studies have shown that mPFC receives intense cholinergic innervation from the basal forebrain and is strongly modulated by acetylcholine (ACh) [26, 44-46]. Notably, cholinergic modulation of the mPFC is severely impaired in neuropathic pain, while activating the cholinergic projection from the nucleus basalis magnocellularis to the mPFC induces antinociceptive effects[47, 48]. These observations prompted us to investigate whether the mPFC *Foxp2*$^{+}$ neurons are modulated by cholinergic innervation.

To determine whether the mPFC *Foxp2*$^{+}$ neurons receive direct monosynaptic cholinergic inputs, rabies virus (RV)-based monosynaptic retrograde tracing was performed (Fig. 6a). Cre-dependent AAV helpers encoding TVA-mCherry and rabies G protein were injected into the PL mPFC of *Foxp2*-Cre mice, followed by EnvA-ΔG rabies virus expressing EGFP injected into the same region 4 weeks later. One week after the RV injection, the virus expression and starter cells were confirmed in the mPFC (Fig. 6a). Brain-wide analysis revealed RV-EGFP labeled neurons in several brain regions, including the basal forebrain, insular cortex, thalamus, ventral hippocampus

342 and basolateral amygdala, while fewer labeled neurons were also observed in hypothalamus, dorsal
343 raphe nucleus and parabrachial nucleus (Fig. 6b and Extended Data Fig. 5a, b). Notably, a
344 substantial number of neurons were labeled with RV-EGFP in basal forebrain, particularly the
345 HDB, with the RV-EGFP labeled neurons distributed from anterior to posterior part of HDB (Fig.
346 6b). Further immunostaining showed that most RV-EGFP labeled neurons HDB also express
347 choline acetyltransferase (ChAT), a marker for cholinergic neurons (Fig. 6c), indicating the direct
348 monosynaptic cholinergic inputs from HDB to the mPFC *Foxp2*$^{+}$ neurons. These results suggest
349 that the mPFC *Foxp2*$^{+}$ neurons receive monosynaptic inputs from the HDB cholinergic neurons.
350
351 To examine the functions of the HDB inputs to the mPFC in pain, Cre-dependent AAVs encoding
352 EYFP or ChR2 were injected into the HDB of the *ChAT*-Cre mice and an optical fiber was
353 implanted above the PL mPFC region to enable specific activation of the HDB^{ChAT}→mPFC circuit
354 (Fig. 6d). The virus expression as well as the fiber implantation were confirmed by *post hoc*
355 histological examination (Fig. 6d). Three weeks after the surgery, VFT and HPT were performed
356 and a significant increase in the VFT was observed in response to optogenetic activation of the
357 circuit (Fig. 6e), indicating reduced mechanical sensitivity of the mice. However, no significant
358 effect was observed in the HPT (Fig. 6e), indicating that the baseline thermal sensitivity is
359 unaffected. To further evaluate the roles of this circuit in chronic pain, the mice were treated with
360 CFA to induce chronic inflammatory pain. VFT and HPT analyses indicated that optogenetic
361 activation of the HDB cholinergic terminals in mPFC significantly alleviated both the mechanical
362 and thermal hypersensitivity in chronic pain, as indicated by increased paw withdrawal threshold
363 and latency (Fig. 6f). Together, these results demonstrate that the mPFC *Foxp2*$^{+}$ neurons receive
364 direct monosynaptic cholinergic innervation from the HDB, which regulates the nociceptive
365 sensitivity in mice.
366
367 **The mPFC *Foxp2*$^{+}$ neurons highly express α4β2 nAChR which facilitates pain relief**
368 Given the critical roles of the cholinergic signaling in pain processing and the innervation of mPFC

369 *Foxp2*$^{+}$ neurons by cholinergic inputs, we next sought to identify the specific acetylcholine
370 receptor (AChR) responsible for modulating the mPFC *Foxp2*$^{+}$ neurons. In the cerebral cortex,
371 there are mainly two types of nicotinic acetylcholine receptors (nAChR), the α7 and the α4β2
372 nAChRs, and two types of muscarinic acetylcholine receptors (mAChR), the M1 and M2
373 receptors[46]. To this end, we performed smFISH analyses for these receptors as well as *Foxp2* and
374 *Oprk1*. The results showed that over 95% of the *Foxp2*$^{+}$ cells express *Chrna4*, the gene encoding
375 the α4 subunit of α4β2 nAChR, while very few express *Chrna7* (Fig. 7a). Further smFISH analysis
376 of *Chrna4* and *Chrnb2*, which encodes the β2 subunit, revealed that around 93% of the *Foxp2*$^{+}$
377 cells are positive for both (Extended Data Fig. 6a), while less than 10% of *Oprk1*$^{+}$ cells express
378 both (Fig. 7b and Extended Data Fig. 6b), indicating the predominant expression of α4β2 nAChR
379 in the *Foxp2*$^{+}$ neurons. smFISH analysis of mAChRs showed that *Chrm1*, encoding the M1
380 receptor, was widely expressed across the mPFC, with expression in nearly all *Foxp2*$^{+}$ and *Oprk1*$^{+}$
381 cells in L6 (Fig. 7c and Extended Data Fig. 6c), while minimal expression of *Chrm2* in *Foxp2*$^{+}$
382 cells were observed (Fig. 7d and Extended Data Fig. 6d). Notably, quantitative analysis revealed
383 the selective expression of the α4β2 nAChRs in *Foxp2*$^{+}$ cells in mPFC L6, with nearly 80% of
384 α4β2 nAChR-expressing cells being *Foxp2*$^{+}$ and only a minority is *Oprk1*$^{+}$ (Fig. 7e). Collectively,
385 these results indicate that while α7 nAChR and M2 expressions are relatively low and M1 is
386 broadly expressed in mPFC, the α4β2 nAChR is highly expressed and enriched in the L6 *Foxp2*$^{+}$
387 neurons of mPFC (Fig. 7f).
388
389 Given the critical roles of the mPFC *Foxp2*$^{+}$ neurons in pain processing and the strong effects of
390 ACh in modulating neuronal activity in mPFC[46], we next asked whether the α4β2 nAChR in mPFC
391 regulates pain. To this end, we bilaterally implanted guided cannula for intracranial drug infusion
392 into the mPFC of WT mice, confirmed by *post hoc* histological examination (Fig. 7g). We first
393 infused artificial cerebrospinal fluid (ACSF) or ABT-594, a specific α4β2 nAChR angonist[27], at
394 different dosages (2.5, 5, and 25 pmol/site) into the mPFC and performed VFT to measure the
395 mechanical sensitivity of the mice. We found that ABT-594 at 5 or 25 pmol per site significantly

396 increase the paw withdrawal threshold in VFT compared to both baseline and the ACSF control
397 (Fig. 7h and Extended Data Fig. 7a), indicating reduced mechanical sensitivity by activating the
398 α4β2 nAChR. Since the antinociceptive effect is sufficiently elicited by the treatment of ABT-594
399 at the dosage of 5 pmol per site, this dosage is used in all the subsequent experiments. Similar
400 antinociceptive effects were observed in the hot plate test (HPT), with increased paw withdrawal
401 latency following ABT-594 treatment (Fig. 7h). To test whether the α4β2 nAChR is also involved
402 in regulating chronic pain, we treated the mice with CFA to induce chronic inflammatory pain. We
403 found that ABT-594 treatment significantly increased the paw withdrawal threshold in VFT and
404 latency in HPT (Fig. 7i), indicating the treatment alleviated mechanical and thermal
405 hypersensitivity in chronic inflammatory pain. However, CPP test revealed no significant effect of
406 ABT-594 on the affective components of pain, although a trend of increased CPP score was
407 observed (Extended Data Fig. 7b), indicating that ABT-594 treatment is not sufficient to relieve
408 the affective components of pain.
409
410 The high levels of α4β2 nAChR expression in the mPFC *Foxp2*$^+$ neurons prompted us to ask
411 whether the antinociceptive effects of ABT-594 depend on activation of the mPFC *Foxp2*$^+$ neurons.
412 To this end, Cre-dependent AAVs encoding mCherry or hM4Di were bilaterally injected into the
413 PL mPFC of the *Foxp2*-Cre mice, followed by guided cannula implantation for intracranial drug
414 delivery (Fig. 7j). The virus expression and the cannula implantation were confirmed by *post hoc*
415 histological examination (Fig. 7j). Three weeks after the surgery, VFT and HPT were performed.
416 In both the mCherry and hM4Di groups, intracranial ABT-594 delivery significantly increased the
417 paw withdrawal threshold in VFT and latency in HPT (Fig. 7k). Notably, systemic administration
418 of CNO, which selectively inhibits hM4Di-expressing mPFC *Foxp2*$^+$ neurons, abolished these
419 effects in the hM4Di group, while no significant changes were observed in the mCherry group
420 (Fig. 7k). These results indicate that the antinociceptive effects of α4β2 nAChR activation are
421 mediated by the mPFC *Foxp2*$^+$ neuron activity.
422

423 Collectively, these results demonstrate that the α4β2 nAChR is highly expressed in the mPFC
424 *Foxp2*$^{+}$ neurons and activation of this receptor is antinociceptive, which depends on the activation
425 of the mPFC *Foxp2*$^{+}$ neurons.

426 **Discussion**

427

428 The present study reveals how the mPFC modulates different dimensions of pain through different
429 thalamic projections and uncovers the critical roles of the cholinergic signaling in mPFC in pain
430 regulation (Fig. 8). We identified *Foxp2* as a marker for the thalamus-projecting neurons in mPFC
431 by neural tracing and smFISH (Fig. 1). *In vivo* recordings showed that these neurons are
432 deactivated in both acute and chronic pain (Fig. 2). Combined cell-type specific and circuit-
433 specific manipulation studies revealed the critical roles of the mPFC *Foxp2*$^{+}$ neurons in regulating
434 sensory and affective pain through discrete thalamic projections (Fig. 3-5). We also showed the
435 cholinergic innervation from HDB and the expression of α4β2 nAChR, which is antinociceptive,
436 in the mPFC *Foxp2*$^{+}$ neurons, underscoring the roles of the HDB^{ChAT}→mPFC^{Foxp2}→thalamus
437 circuit in pain regulation (Fig. 6, 7).

438

439 The cerebral cortex is organized into layers with intermingled distribution of projection neurons
440 that target diverse brain regions[37]. While our understanding of cortical circuitry has predominantly
441 emerged from sensory cortices[19, 49], recent studies have revealed some distinct features of cellular
442 organization and connections of the mPFC [19, 35, 36, 50]. Notably, we found that *Ntsr1*, a widely used
443 marker for L6 CT neurons in sensory cortex and motor cortex[22, 33, 34], is broadly expressed across
444 multiple layers in mPFC. The expression of *Foxp2* has been well described in developing brain
445 and the sensory cortex of adult brain[37-40], but it is not clear whether *Foxp2* is specifically expressed
446 in the L6 CT neurons in mPFC of adult mice. Our smFISH results showed that the *Foxp2*
447 expression is restricted in the glutamatergic neurons of the deep layers in mPFC, mostly in L6, and
448 has few overlaps with the markers for other projection neurons such as IT, ET and NP neurons
449 (Fig. 1c-g). Retrograde labeling further confirmed that *Foxp2* specifically labels the mPFC neurons
450 projecting to thalamus, but not those to cPFC, PAG, NAc or BLA (Fig. 1a, b and Extended Data
451 Fig. 1c-e). Consistently, axon terminal labeling revealed that the mPFC *Foxp2*$^{+}$ neurons almost
452 exclusively project to thalamus with much weaker signals in medial striatum, and no detectable
453 signal in NAc, BLA and PAG (Fig. 1h, i and Extended Data Fig. 1f-m). Interestingly, it is reported

that a subset of *Foxp2*$^{+}$ neurons in PFC project to VTA[39], but we did not observe axon-labeling signals in VTA (Extended Data Fig. 1m). One possible explanation is that the reported VTA-projecting *Foxp2*$^{+}$ neurons are mainly located in the ventral part of PFC, especially the dorsal peduncular nucleus (DPn) which show different projection patterns from that of the mPFC[51]. Moreover, we observed limited number of neurons in L5 that express *Foxp2* and found that these neurons do not express markers of IT, ET and NP neurons in mPFC (Fig. 1e, g), consistent with tracing results. Our study therefore provides multiple lines of evidence supporting *Foxp2* as a specific marker for the thalamus-projecting neurons in mPFC.

Substantial evidence supports the involvement and critical roles of mPFC in pain regulation[8, 10] and previous studies have uncovered the roles of the mPFC L5 ET neurons projecting to PAG, a key node for the descending modulatory pathway that dictates the processing of noxious information in the spinal cord[16, 17]. However, although the functions of the mPFC IT neurons that project to BLA and striatum have also been indicated[8, 9], it is much less clear how the mPFC modulates the processing of noxious information in the brain, particularly for the roles of the output to thalamus[30]. Thalamus is a key hub for integrating noxious information and regulates multiple aspects of pain[5]. We showed that the thalamus-projecting *Foxp2*-expressing neurons in mPFC are deactivated in response to various noxious stimulation and recover gradually after the removal of the stimuli (Fig. 2), indicating the involvement of these neurons in both acute and chronic pain. In contrast to the motor cortex to thalamus circuit that mainly involved in affective pain[22], we found that persistent inactivation of the mPFC *Foxp2*$^{+}$ neurons sensitizes nociception (Fig. 3a-c), while activation relieves both sensory and affective components of pain (Fig. 3d-h), demonstrating the crucial functions of the mPFC CT neurons in the endogenous pain relief pathway. Interestingly, short-term chemogenetic inhibition of the mPFC *Foxp2*$^{+}$ neurons has few effects on pain-related behaviors (Extended Data Fig. 4a-d). Indeed, the organization of the mPFC-thalamus connection is consistent with the canonical model, in which the L6 CT neurons as “modulators” project to thalamus with low initial release probability, but are able to evoke robust firing in thalamus by

strongly facilitating synapses[52, 53]. Our results indicate that short-term inhibition of the mPFC *Foxp2*$^+$ neurons may not induce adaptive alterations in the mPFC-thalamus connection and long-term adaptations in this pathway are responsible for the sensitized nociceptive responses induced by persistent inhibition of the mPFC *Foxp2*$^+$ neurons.

Our study also delineates the circuit mechanism underlying the roles of the mPFC *Foxp2*$^+$ neurons in regulating pain. The thalamus receives nociceptive information directly from the spinothalamic tract and is widely connected to other brain regions[54]. It has been proposed that the lateral thalamic system mediates discriminative features of pain, while the medial system mediates the emotional aspects of pain[5]. Our results show PTN, MD and VM of thalamus as the major targets of the mPFC *Foxp2*$^+$ neurons (Fig. 1h, i) and reveal the critical roles of mPFC in modulating the nociceptive processing by these thalamic projections (Fig. 4, 5). We found that while the projection of the mPFC *Foxp2*$^+$ neurons to PTN regulates both sensory and affective pain, the projection to MD relieves affective pain and the one to VM regulates coping behaviors specifically (Fig. 4, 5). These findings support the idea that segregated circuit mechanisms are responsible for different dimensions of pain[5, 20]. Our results reveal PTN, which is a relatively less studied region with the functions and circuits remained to be fully characterized, as a master hub in the medial thalamus for regulating both the sensory and affective aspects of pain. Future study is needed to further clarify the circuit mechanism underlying the critical roles of PTN in pain regulation. In summary, our study reveals the critical roles and the segregated circuit mechanisms of mPFC in governing the nociceptive processing in the thalamus.

The mPFC is broadly connected to a wide range of brain regions[19]. While the strengthened input from BLA to the inhibitory neurons in mPFC has been proposed to be a key mechanism underlying the functional deactivation of mPFC in chronic pain[17], the contributions of other inputs are far from fully understood. The mPFC receives dense cholinergic innervation from the basal forebrain and expresses high levels of cholinergic receptors[26, 46]. It is reported that the ACh receptors are

expressed in a layer-specific manner, with some expression of α4β2 nAChR in the inhibitory neurons of L2/3 and much higher expression in the excitatory neurons in L5/6 of mPFC[44]. Consistently, our results showed that the expression of α4β2 nAChR is enriched in deep layers of mPFC and more specifically in the L6 CT neurons, while the α7 nAChR is expressed in IT neurons (Fig. 7a-f and Extended Data Fig. 6). We further revealed that the cholinergic inputs to the *Foxp2*$^+$ neurons are from the basal forebrain, particularly the HDB, by monosynaptic retrograde tracing (Fig. 6a-c and Extended Data Fig. 5). Our study thus revealed the cell-type specific expression patterns of the AChRs in mPFC as well as the cholinergic inputs to the mPFC L6 CT neurons.

Cholinergic signaling has been extensively studied in the context of pain and analgesia, with significant insights into its roles in the peripheral, spinal cord and descending modulation pathway[55-58]. However, the functions and circuit mechanisms of cholinergic system in the brain in nociceptive processing are not fully understood[47]. While cholinergic input is known to be essential for the mPFC functions such as attention and cognition, its role in pain regulation is less clear[26, 45, 46]. Notably, cholinergic signaling in the mPFC is markedly impaired in neuropathic pain models[48], and activation of cholinergic projections from the nucleus basalis magnocellularis to the mPFC has been shown to produce antinociceptive effects[47]. Our study revealed that the mPFC *Foxp2*$^+$ neurons receive cholinergic inputs from the HDB, which regulates the sensory aspects of pain (Fig. 6d-f). We also found that targeting the α4β2 nAChR in mPFC with a specific agonist ABT-594, which is antinociceptive through systemic administration or brainstem injection[27], alleviates pain (Fig. 7g-i). Importantly, this antinociceptive effect requires the activity of the mPFC *Foxp2*$^+$ neurons (Fig. 7j, k). Notably, desensitization is an important property of the nAChRs, and the receptors are desensitized in response to high concentration or affinity of agonist[59]. In our study, we used a relatively low concentration of agonist that has been found to activate the neurons in brainstem[27]. On the other hand, the L6 pyramidal neurons in cortex express *Chrna5*, which encodes an accessory subunit of the α5-containing α4β2 nAChR[60]. This receptor complex could increase conductance and prolong inward currents in response to persistent nicotine application and is

important for the tonic effects of ACh[46, 61]. Thus, the α4β2 nAChR in *Foxp2*$^{+}$ neurons could play an important role in maintaining the baseline neuronal activity and activating the endogenous pain relief pathway. While further studies are still needed to fully elucidate how the cholinergic inputs from HDB modulate the mPFC activity in chronic pain, our results support the crucial role of the cholinergic signaling in the mPFC *Foxp2*$^{+}$ neurons in pain processing.

Besides the cholinergic inputs, we also revealed other monosynaptic inputs to the mPFC L6 CT neurons, including the IC and BLA (Extended Data Fig. 5), which are important for pain processing[5, 62]. It is well-known that in chronic pain, BLA sends strengthened feedforward inhibition to the L5 ET neurons of mPFC that further project to the PAG to regulate pain[17]. However, the effects of the BLA inputs to the L6 CT neurons are unknown. Future studies will reveal the respective contributions of these specific inputs.

Collectively, our study uncovers the crucial roles of the mPFC in modulating sensory and affective aspects of pain through the discrete HDB^{ChAT}→mPFC^{Foxp2}→thalamic nuclei circuits and raises the possibility of managing chronic pain by targeting the mPFC L6 CT neurons.

Materials and Methods

EXPERIMENTAL MODEL AND STUDY PARTICIPANT DETAILS

Animals

All experiments were conducted in accordance with the National Institutes of Health Guide for Care and Use of Laboratory animals and approved by the Institutional Animal Care and Use Committee (IACUC) of Boston Children's Hospital and Harvard Medical School. The wild-type C57BL/6 mice (Jax, 000664), B6.Cg-*Foxp2*$^{tm1.1(cre)Rpa}$/J mice (Jax, 030541) and B6.129S6-*Chat*$^{tm2(cre)lowl}$/J mice (Jax, 006410) were purchased from Jackson Laboratory. Mice were housed with littermates (3-5 mice/cage) in 12-hr light/dark cycle (light on from 7:00 to 19:00) with food and water *ad libitum* unless otherwise specified. Ambient temperature (23-25°C) and humidity (55-62%) were automatically controlled. For the present study, 2-4-month-old male mice were used and all mice were randomly assigned into different groups.

METHODS DETAILS

Single molecule Fluorescence *in situ* hybridization (smFISH) and immunofluorescence (IF) staining

Mice were euthanized by inhalation of CO_2 and transcardially perfused with PBS and 4% paraformaldehyde (PFA) before the brains were collected and fixed in 4% PFA at 4 ℃ overnight, followed by dehydration in 30% sucrose solution for 3 days. The brains were then frozen in Optimal Cutting Temperature embedding media (Sakura, #4583) and coronal sections (14 μm for smFISH and 30 μm for IF) were cut using a cryostat (Leica, #CM3050S). The smFISH was performed using a RNAscope Fluorescent Multiplex Assay kit (Advanced Cell Diagnostics, ACD) following the manufacturer's instruction. Briefly, the brain slices were fixed with fixed with 4% PFA and washed with PBS, then dehydrated with ethanol and treated with hydrogen peroxide. The samples were then treated with the target retrieval reagents and protease for 10 minutes, after which the samples were hybridized with the probes in 40°C for 2 hours. Then the signals were amplified using the reagents included in the kit, followed by the labeling of relative channels with the TSA fluorophores. The samples were treated with the included blocking buffer before proceeding to

DAPI staining and imaging. For the combined smFISH with CTB retrograde tracing, the brain samples were prepared from the mice with CTB injected into the relative regions. The samples were treated following the manufacturer's instruction as described above till the labeling with TSA fluorophore without being treated with the blocking buffer. The samples were then directing stained with DAPI and the images were captured immediately. Probes (ACD) used were as followed: Foxp2 (Cat. No. 428791-C1; Cat. No. 428791-C2); Slc17a7 (Cat. No. 416631-C3); Gad1 (Cat. No. 400951-C2); Ctgf (Cat. No. 314541-C1); Etv1 (Cat. No. 557891-C3); Oprk1 (Cat. No. 316111-C1; Cat. No. 316111-C2); Tshz2 (Cat. No. 431061-C3); Pou3f1 (Cat. No. 436421-C2); Chrna4 (Cat. No. 429871-C3); Chrna7 (Cat. No. 465161-C2); Chrnb2 (Cat. No. 449231-C2); Chrm1 (Cat. No. 495291-C2); Chrm2 (Cat. No. 495311-C1).

For IF staining, the brain slices were washed in PBS twice for 10 min, followed by incubation in blocking buffer (5% goat serum, 5% BSA and 0.1% Triton X-100 in PBS) for 40 min at room temperature. The samples were then incubated at 4°C for 24 h with primary antibody diluted in PBS containing 1% BSA. After the incubation, the samples were washed three times with washing buffer (0.1% Tween-20 in PBS) and incubated with the Alexa Fluor conjugated secondary antibodies for 2 h at room temperature. The sections were washed for three times, mounted and imaged using a Zeiss LSM800 confocal microscope or Keyence BZ-X810 microscope. Antibodies used were as followed: rabbit anti-cFos (1:1000, Synaptic Systems, #226003), rabbit anti-ChAT (1:1000, Milliopore, #ZRB1012-25UL), Donkey anti-rabbit Alexa Fluor 488 (Thermo Scientific, #A21206), Donkey anti-rabbit Alexa Fluor 568 (Thermo Scientific, # A10042).

Stereotaxic surgeries

All stereotaxic surgeries were performed using a small-animal stereotaxic instrument (David Kopf Instruments, model 940) under general anesthesia by isoflurane ($0.8\,\mathrm{l\,min^{-1}}$; isoflurane concentration 1.5%) in oxygen. A feedback heater was used to maintain the body temperature of the mice. The eyes of the mice were kept moist using ophthalmic ointment throughout the surgery.

A small craniotomy above the target brain region was performed using a dental drill. The viruses and CTB were injected into the target regions using a glass micropipette (10-20 μm in diameter at the tip) that was connected to a nanoliter injector (Nanoject III, Drummond Scientific, #3-200-207). For each site, 120 nl of viruses were injected at a flow rate of 1 $\mathrm{nl\,s^{-1}}$ unless otherwise specified, allowing an additional 5 min for viral particles to diffuse before the pipette was slowly withdrawn. After the withdrawal, the wound was sutured and the mice were allowed to recover in a warm blanket before being transferred to the housing cages. The mice were treated with meloxicam (Covetrus, Cat. No. 049756) subcutaneously daily for 3 days and monitored for another 2 days.

The coordinates of viral injection and implantation sites are based on previous literature and The Mouse Brain in Stereotaxic Coordinates (third edition) relative to the bregma (anterior-posterior, mediolateral, dorsoventral axis in mm): PL (1.94, 0.45, -2.50), PTN (-0.46, 0.30, -3.70), MD (-1.22, 0.50, -3.20), VM (-1.34, 0.75, -4.20), PAG (-4.75, 0.55, -2.70), NAc (+1.20, 0.60, 4.50), BLA (-1.34, 2.90, -4.50), HDB (-0.10, 1.45, -5.50).

Chemogenetic and optogenetic manipulations

For chemogenetic manipulations of the PL mPFC *Foxp2*$^{+}$ neurons, AAV5-hSyn-DIO-mCherry, AAV5-hSyn-DIO-hM4D(Gi)-mCherry or AAV5-hSyn-DIO-hM3D(Gq)-mCherry was bilaterally injected into the PL mPFC of *Foxp2*-Cre mice. The behavioral assays were performed 3 weeks later, and the mice were intraperitoneally injected with CNO (Cayman, Cat# 16882) at 1 mg/kg (for activation) or 5 mg/kg (for inactivation) in saline 20 min before each behavioral test as previously described[63, 64]. For persistent chemogenetic inactivation, the mice were intraperitoneally injected with CNO twice per day for 5 consecutive days. For persistent inactivation of the mPFC *Foxp2*$^{+}$ neurons, rAAV2/9-hSyn-DIO-EYFP or rAAV2/9-hSyn-DIO-TeNT-EYFP was bilaterally injected into the mPFC of *Foxp2*-Cre mice and behavioral assays were performed 5 weeks later.

634

635 For optogenetic activation of the terminals of PL mPFC *Foxp2*$^{+}$ neurons, rAAV2/9-EF1a-DIO-
636 EYFP or rAAV2/9-EF1a-DIO-ChR2-EYFP was bilaterally injected into the PL mPFC of *Foxp2*-
637 Cre mice, followed by the bilateral implantation of optical cannulas (diameter: 200 μm; N.A., 0.37;
638 length, 4.0 mm; Inper Inc., China) 100 μm above the PTN/MD/VM region and secured with dental
639 cement (Parkell, no. S380). For optogenetic activation of the cholinergic inputs to PL mPFC, the
640 same viruses were injected into the HDB region of *ChAT*-Cre mice, and the optical cannulas were
641 implanted above the PL mPFC. For all optogenetic manipulation, the mice were connected to the
642 optical fiber for acclimation for 3 days before the behavioral tests and the light pulses (473 nm,
643 1.5 mW at the tip of the fiber, 20 Hz, 5-ms pulse) at 10-s ON/OFF cycle were generated by a 473-
644 nm laser (OEM laser/OptoEngine) and used throughout the behavioral tests controlled by a
645 waveform generator (Keysight).

646

647 **Neuronal tracing**

648 For CTB retrograde tracing, 120 nl of CTB-555 was unilaterally injected into the MD, mPFC,
649 PAG, NAc or amygdala in individual mice, respectively. The brain tissues were collected 1 week
650 later for smFISH. For specific axon labeling of the mPFC *Foxp2*$^{+}$ neurons, pAAV1-hSyn-DIO-
651 mGFP-Synaptophysin-mRuby was unilaterally injected into the mPFC of *Foxp2*-Cre mice. For
652 specific axon labeling of the HDB cholinergic neurons, the same virus together with rAAV2/9-
653 ChAT-Cre-EGFP was injected into the HDB region of WT mice. The brain tissues were collected
654 3 weeks after the surgery.

655

656 For monosynaptic retrograde rabies tracing, 150 nl mixture of AAV helpers (rAAV2/9-EF1a-DIO-
657 mCherry-TVA and rAAV2/9-EF1a-DIO-RVG) was unilaterally injected into the PL mPFC of the
658 *Foxp2*-Cre mice. Four weeks later, the same mice were injected with 250 nl of rabies virus (RV-
659 ENVA-ΔG-EGFP) to the same location. The brain tissues were collected 7 days later for imaging
660 and examination.

661

662 **Intracranial drug delivery**

663 For intracranial drug delivery into the PL mPFC, the double cannula (Guide cannula: M3.5, C.C
664 1.0mm, C=2.5mm; Injector: G1=0.5mm; Dummy cannula: G2=0, mates with M3.5; RWD Life
665 Science) with dust caps targeting both sides were directly implanted 0.5 mm above the PL mPFC
666 and were secured with dental cement. Two weeks later, an injector (G2=0, mates with M3.5; RWD
667 Life Science) filled with mineral oil and ABT-594 (Cayman Chemical, Cat. No. 22822) was
668 connected to a pump (RWD Life Science) to slowly infuse the drug into both sides of mPFC (200
669 nl/site, 5 min) and 5 min were allowed for drug diffusion before the injector was slowly removed.
670 The behavioral tests were performed another 5 min later. For intracranial drug delivery combined
671 with chemogenetic inhibition, AAV5-hSyn-DIO-mCherry or AAV5-hSyn-DIO-hM4D(Gi)-
672 mCherry was bilaterally injected into the mPFC, followed by the implantation of the double
673 cannula. Three weeks later, the behavioral tests were performed 20 min after CNO injection (i.p.)
674 and 5 min after ABT594 infusion (intracranially).

675

676 ***In vivo* miniscopic calcium imaging and data processing**

677 To probe the activity of the PL mPFC *Foxp2*$^{+}$ neurons in response to pain, *in vivo* miniscopic
678 calcium imaging was performed as previously described[64, 65]. Firstly, AAV1-hSyn-DIO-jGCaMP7s
679 was unilaterally injected into the PL mPFC of the *Foxp2*-Cre mice. Two weeks later, the mice were
680 anesthetized and fixed on a stereotaxic frame. The skull above the target region was carefully
681 removed using a dental drilling and the brain tissue above the target region was aspirated using a
682 27-gauge needle with a blunt tip. Then an integrated GRIN lens (diameter 1.0 mm, length 4.0 mm;
683 Inscopix) connected to a data acquisition system for monitoring the calcium signal was slowly
684 lowered (~100 μm/min) down to 300 μm above the target region. The GRIN lens was further
685 inserted to obtain an optimal field of view to image calcium signals and then the GRIN lens was
686 secured to the mice's skull with dental cement attached to a baseplate cover for protection. Saline
687 was continuously added to avoid bleeding or drying of the tissue during the surgery. After the

surgery, the mice were individually housed for 2 weeks before being used in imaging experiments. Prior to calcium imaging recording, the mice were connected to the microscope through the head-fixed baseplate and acclimated to the handling of the experimenter and the testing chamber for 30 min each day for 3 days. On the day of data acquisition, the mice were connected to the microscope and allowed to move freely in the testing chamber. After 10 min of acclimation, the calcium images were obtained for 20-30 min using nVoke system (Inscopix) at 20 Hz with 0.6-1.2 mW of LED power and 1.5 of gain. For individual mice, the imaging parameters were kept consistent across days.

For tail pinch stimulation, after acclimatation the mice were placed in the testing chamber without stimulation for 2 min and then an alligator clip was applied to the tail for 1 min, after which the clip was removed and the mice were allowed to recover for 9 min, and the calcium signals were recorded during the entire process. For formalin stimulation, after acclimatation the mice were recorded in the testing chamber without stimulation for 5 min, and then 20 μl of formalin was injected to the plantar of the mice, after which the mice were recorded for another 30 min in the chamber.

To detect the spontaneous activity of the neurons, the mice were acclimated to the microscope and testing environment with fixed brightness, temperature and noise level one hour before the recordings. To avoid the potential effects of light-dark cycle on the neuronal activity, all the recordings were performed in the afternoon and at the fixed time points for each individual animal. After the acclimation, the calcium activities were recorded for 15 minutes for the baseline. Then the mice were subjected to saline or CFA injection under isoflurane anesthesia. One or seven days after the injection, the calcium activities were recorded again at the same time point after acclimation without any additional stimulation.

For data processing, the calcium traces were extracted and analyzed using the Inscopix Data

Processing Software (version 1.9, Inscopix). The raw images were cropped, temporally downsampled (2x), spatially downsampled (2x), and further spatially filtered as well as motion-corrected using the default settings. The signals of putative individual cells were identified using an extended constrained non-negative matrix factorization (CNMF-E) algorithm and were normalized to ΔF over noise (settings: cell diameter: 8 pixels; minimum pixel correlation: 0.85; minimum peak-to-noise ratio: 15). The identified individual cells were then manually checked to be included based on their anatomy (size, shape, location), signal-to-noise ratio as well as overlap in spatial location and signal with other cells. The calcium signal traces were further deconvoluted using OASIS (online active set method to infer spikes) methods to detect the potential calcium transients with the default noise ranges and spike signal-to-noise ratio of 8.0. Across the different days of recording for chronic pain, we first analyzed the calcium images to identify individual neurons in each recording and compared the spontaneous calcium activities of all the identified neurons among different days. Then the identified individual neurons were longitudinally registered with minimum correlation of 0.9 and the matched neurons were further manually checked to be the same neurons across different days based on the locations and other visible landmarks (such as blood vessels).

To identify the neurons with significant change in the firing rate in response to tail pinch stimulation, the calcium traces were extracted and deconvoluted using OASIS to identify the calcium transients. We pooled together the identified transients of 2 min before and 1 min during the tail pinch stimulation, and used a permutation method to create 10,000 shuffled distributions of the transients. Then the shuffled transient change was calculated by subtracting shuffled 0-2 min from that of the 3rd min. The neurons with actual transient change ranked higher than 99.5th percentile of the shuffled transient change were classified as activity-increased neurons, and those ranked lower than 0.5th percentile were classified as activity-decreased neurons. For formalin test, the calcium signals of -5 min to 0 min and that of 0 min to 5 min were compared. For CFA-induced chronic inflammatory pain, the calcium signals of the baseline, CFA D1 and CFA D7 were

742 compared using the same method.

743

744 **Behavioral assays**

745 ***von Frey test***. The mechanical sensory threshold of the mice was measured with a series of von
746 Frey filaments (ranging from 0.04-2.0 g, Stoelting) using the Up-Down method as previously
747 described[66]. Briefly, the mice were placed in a plastic chamber with a metal mesh floor and allowed
748 to move freely. After 20 min of acclimation of the mice, the von Frey filaments were applied to
749 the mid-plantar surface of the hindpaw through the mesh floor and kept for 2 s, or until there was
750 a positive response (paw withdrawal, flinching, licking or shaking). To avoid the potential false
751 positive responses caused by movement, the measurement was conducted again if a positive
752 response was followed by other voluntary behaviors such as locomotion, exploratory or grooming
753 behaviors.

754

755 ***Hot plate test***. The hot plate test was used to measure thermal nociception of the mice. After being
756 acclimated in the testing room for 20 min, the mice were placed on a hot plate (Ugo Basile) set at
757 52 ℃ and the latencies to flinching or licking of hindpaws were measured. All animals were tested
758 for 3 times with a minimum interval of 30 min. To avoid tissue injury, a cutoff latency was set at
759 30 s for the test.

760

761 ***Formalin test***. Formalin test was performed as previously described[42]. Briefly, 20 μl of 2%
762 formalin (Sigma-Aldrich, HT5011-1CS) was injected subcutaneously into the plantar surface of
763 one hind paw of the mice with a 30-gauge syringe as quickly as possible. The licking behaviors
764 were measured for 45 min starting the injection of formalin and the licking duration were
765 calculated in 5-min bins. The licking duration of the mice during phase 1 (defined as 0 - 5 min
766 after formalin injection) and phase 2 (defined as 15 - 45 min after formalin injection) were analyzed.

767

768 ***Complete Freund's adjuvant (CFA) injection.*** For CFA-induced inflammatory pain, 15 μl of CFA

(Sigma, F5881-10ML) was subcutaneously injected into the plantar surface of the right hind paw of the mice under brief isoflurane anesthesia.

Conditioned place preference. The conditioned place preference test was used to measure the negative affection of pain and the effects of pain relief as previously described[64]. The testing apparatus consists of an infrared photobeam detectors for tracking the mice trajectories and two compartments, one of which is with rod style floor and the other one is with grid style floor (Med Associates). For chemogenetic manipulations, individual mice were placed in the chamber and allowed to freely explore the entire apparatus for 30 min (pretest) on day 1. On day 2-4, mice injected with saline were placed in the compartment with grid floor (unconditioned compartment) for 30 min in the morning, while mice injected with CNO were placed in the opposite compartment with rod floor (conditioned compartment) of the same apparatus for 30 min in the afternoon (with a minimum interval of 6 h between the two conditioning). On day 5, like day 1, the mice were placed in the chamber and allowed to freely explore the entire apparatus for 30 min (posttest). For optogenetic activation, the pretest and posttest on the first and last day were similarly performed. On day 2-4, the mice were connected with optical fiber without light stimulation and placed in the compartment with grid floor for 30 min in the morning, and in the afternoon, the mice were connected with the optical fiber with light stimulation as described above, and placed in the compartment with rod floor for 30 min. For ABT-594 treatment, the pretest and posttest on the first and last day were similarly performed. On day 2-4, the mice were intracranially injected with ACSF and placed in the compartment with grid floor for 30 min in the morning, and in the afternoon, the mice were injected with ABT-594 and placed in another compartment for 30 min. To calculate the CPP score, the time that mice spent in the conditioned compartment during pretest was subtracted from the one during posttest.

Statistics

The mice were randomly assigned to the groups and the investigators were blind to the allocation

of the groups or the outcome assessment. No statistical method was used to predetermine the sample size, but our sample sizes are similar to those reported in previous publications. Mice that, after histological inspection, had the location of the viral injection (reporter protein), cannula implantation, or the optic fiber(s) outside the area of interest were excluded. The data are presented as means ± SEM. Statistical analyses were performed using GraphPad Prism (version 8.0). Student's t-test and one-way or two-way RM ANOVA test with Tukey's or Sidak's *post hoc* multiple comparisons were applied to determine statistical differences. Statistical significance was set at $^{*}P < 0.05$, $^{**}P < 0.01$, $^{***}P < 0.001$.

Data availability

All data generated or analyzed during this study are included in this article and its Supplementary Information files.

Code availability

Data and custom MATLAB code are available upon request.

Acknowledgements

We thank the support of Mouse Behavior Core of Harvard Medical School and its director Dr. Barbara Caldarone. We thank Dr. Zhengdong Zhao for the help in using *in vivo* miniscopic calcium recording. This project was supported by the Open Philanthropy Foundation, the National Institutes of Health (1R01DA050589), and the HHMI. Y.Z. is an investigator of the Howard Hughes Medical Institute. This article is subject to HHMI's Open Access to Publications policy. HHMI lab heads have previously granted a nonexclusive CC BY 4.0 license to the public and a sublicensable license to HHMI in their research articles. Pursuant to those licenses, the author-accepted manuscript of this article can be made freely available under a CC BY 4.0 license immediately upon publication.

Author information

Authors and Affiliations

Howard Hughes Medical Institute, Boston Children's Hospital, Boston, MA, USA
Guoguang Xie, Yiqiong Liu, Xuetao Qi, Aritra Battatrajee, Chao Zhang & Yi Zhang

Program in Cellular and Molecular Medicine, Boston Children's Hospital, Boston, MA, USA
Guoguang Xie, Yiqiong Liu, Xuetao Qi, Aritra Battatrajee, Chao Zhang & Yi Zhang

Division of Hematology/Oncology, Department of Pediatrics, Boston Children's Hospital, Boston, MA, USA
Guoguang Xie, Yiqiong Liu, Xuetao Qi, Aritra Battatrajee, Chao Zhang & Yi Zhang

Department of Genetics, Harvard Medical School, Boston, MA, USA
Yi Zhang

Harvard Stem Cell Institute, Boston, MA, USA
Yi Zhang

Contributions

Y.Z. conceived the project; G.X. designed the experiments; G.X. and Y.L. performed the experiments; X.Q. and G.X. analyzed the calcium imaging results; A.B. acquired the *Foxp2*-Cre

mouse line; C.Z. helped to analyze the results. All authors are involved in data interpretation; G.X. and Y.Z. wrote the manuscript with input from all authors.

Corresponding author

Correspondence to Yi Zhang.

Competing interests

The authors declare no competing interest.

References

1. Raja, S.N.*, et al.* The revised International Association for the Study of Pain definition of pain: concepts, challenges, and compromises. *Pain* **161**, 1976-1982 (2020).
2. Treede, R.D.*, et al.* Chronic pain as a symptom or a disease: the IASP Classification of Chronic Pain for the International Classification of Diseases (ICD-11). *Pain* **160**, 19-27 (2019).
3. Kang, Y., Trewern, L., Jackman, J., McCartney, D. & Soni, A. Chronic pain: definitions and diagnosis. *BMJ* **381**, e076036 (2023).
4. Cohen, S.P., Vase, L. & Hooten, W.M. Chronic pain: an update on burden, best practices, and new advances. *Lancet* **397**, 2082-2097 (2021).
5. Kuner, R. & Kuner, T. Cellular Circuits in the Brain and Their Modulation in Acute and Chronic Pain. *Physiol Rev* **101**, 213-258 (2021).
6. Descalzi, G., Ikegami, D., Ushijima, T., Nestler, E.J., Zachariou, V. & Narita, M. Epigenetic mechanisms of chronic pain. *Trends Neurosci* **38**, 237-246 (2015).
7. Mercer Lindsay, N., Chen, C., Gilam, G., Mackey, S. & Scherrer, G. Brain circuits for pain and its treatment. *Sci Transl Med* **13**, eabj7360 (2021).
8. Tan, L.L. & Kuner, R. Neocortical circuits in pain and pain relief. *Nat Rev Neurosci* **22**, 458-471 (2021).
9. Kummer, K.K., Mitric, M., Kalpachidou, T. & Kress, M. The Medial Prefrontal Cortex as a Central Hub for Mental Comorbidities Associated with Chronic Pain. *Int J Mol Sci* **21** (2020).
10. Ong, W.Y., Stohler, C.S. & Herr, D.R. Role of the Prefrontal Cortex in Pain Processing. *Mol Neurobiol* **56**, 1137-1166 (2019).
11. Kuner, R. & Flor, H. Structural plasticity and reorganisation in chronic pain. *Nat Rev Neurosci* **18**, 20-30 (2016).
12. Apkarian, A.V.*, et al.* Chronic back pain is associated with decreased prefrontal and thalamic gray matter density. *J Neurosci* **24**, 10410-10415 (2004).
13. Seminowicz, D.A. & Moayedi, M. The Dorsolateral Prefrontal Cortex in Acute and Chronic Pain. *The journal of pain* **18**, 1027-1035 (2017).
14. Moisset, X. & Bouhassira, D. Brain imaging of neuropathic pain. *NeuroImage* **37 Suppl 1**, S80-88 (2007).
15. Ji, G. & Neugebauer, V. Pain-related deactivation of medial prefrontal cortical neurons involves mGluR1 and GABA(A) receptors. *J Neurophysiol* **106**, 2642-2652 (2011).
16. Wang, G.Q.*, et al.* Deactivation of excitatory neurons in the prelimbic cortex via Cdk5 promotes pain sensation and anxiety. *Nat Commun* **6**, 7660 (2015).
17. Huang, J.*, et al.* A neuronal circuit for activating descending modulation of neuropathic pain. *Nat Neurosci* **22**, 1659-1668 (2019).
18. Cheriyan, J. & Sheets, P.L. Altered Excitability and Local Connectivity of mPFC-PAG Neurons in a Mouse Model of Neuropathic Pain. *J Neurosci* **38**, 4829-4839 (2018).
19. Anastasiades, P.G. & Carter, A.G. Circuit organization of the rodent medial prefrontal cortex. *Trends Neurosci* **44**, 550-563 (2021).
20. Ma, Q. A functional subdivision within the somatosensory system and its implications for pain research. *Neuron* **110**, 749-769 (2022).
21. Gustin, S.M., Peck, C.C., Wilcox, S.L., Nash, P.G., Murray, G.M. & Henderson, L.A. Different pain, different brain:

thalamic anatomy in neuropathic and non-neuropathic chronic pain syndromes. *J Neurosci* **31**, 5956-5964 (2011).

22. Gan, Z.*, et al.* Layer-specific pain relief pathways originating from primary motor cortex. *Science* **378**, 1336-1343 (2022).

23. Meda, K.S.*, et al.* Microcircuit Mechanisms through which Mediodorsal Thalamic Input to Anterior Cingulate Cortex Exacerbates Pain-Related Aversion. *Neuron* **102**, 944-959 e943 (2019).

24. Spellman, T., Svei, M., Kaminsky, J., Manzano-Nieves, G. & Liston, C. Prefrontal deep projection neurons enable cognitive flexibility via persistent feedback monitoring. *Cell* **184**, 2750-2766 e2717 (2021).

25. Lui, J.H.*, et al.* Differential encoding in prefrontal cortex projection neuron classes across cognitive tasks. *Cell* **184**, 489-506 e426 (2021).

26. Ballinger, E.C., Ananth, M., Talmage, D.A. & Role, L.W. Basal Forebrain Cholinergic Circuits and Signaling in Cognition and Cognitive Decline. *Neuron* **91**, 1199-1218 (2016).

27. Bannon, A.W.*, et al.* Broad-spectrum, non-opioid analgesic activity by selective modulation of neuronal nicotinic acetylcholine receptors. *Science* **279**, 77-81 (1998).

28. Pan, Q.*, et al.* Representation and control of pain and itch by distinct prefrontal neural ensembles. *Neuron* **111**, 2414-2431 e2417 (2023).

29. Li, M., Zhou, H., Teng, S. & Yang, G. Activation of VIP interneurons in the prefrontal cortex ameliorates neuropathic pain aversiveness. *Cell Rep* **40**, 111333 (2022).

30. Harris, K.D. & Shepherd, G.M. The neocortical circuit: themes and variations. *Nat Neurosci* **18**, 170-181 (2015).

31. Hodge, R.D.*, et al.* Conserved cell types with divergent features in human versus mouse cortex. *Nature* **573**, 61-68 (2019).

32. Harris, J.A.*, et al.* Hierarchical organization of cortical and thalamic connectivity. *Nature* **575**, 195-202 (2019).

33. Sundberg, S.C., Lindstrom, S.H., Sanchez, G.M. & Granseth, B. Cre-expressing neurons in visual cortex of Ntsr1-Cre GN220 mice are corticothalamic and are depolarized by acetylcholine. *J Comp Neurol* **526**, 120-132 (2018).

34. Olsen, S.R., Bortone, D.S., Adesnik, H. & Scanziani, M. Gain control by layer six in cortical circuits of vision. *Nature* **483**, 47-52 (2012).

35. Bhattacherjee, A., Djekidel, M.N., Chen, R., Chen, W., Tuesta, L.M. & Zhang, Y. Cell type-specific transcriptional programs in mouse prefrontal cortex during adolescence and addiction. *Nat Commun* **10**, 4169 (2019).

36. Bhattacherjee, A., Zhang, C., Watson, B.R., Djekidel, M.N., Moffitt, J.R. & Zhang, Y. Spatial transcriptomics reveals the distinct organization of mouse prefrontal cortex and neuronal subtypes regulating chronic pain. *Nat Neurosci* **26**, 1880-1893 (2023).

37. Tasic, B.*, et al.* Shared and distinct transcriptomic cell types across neocortical areas. *Nature* **563**, 72-78 (2018).

38. Hisaoka, T., Nakamura, Y., Senba, E. & Morikawa, Y. The forkhead transcription factors, Foxp1 and Foxp2, identify different subpopulations of projection neurons in the mouse cerebral cortex. *Neuroscience* **166**, 551-563 (2010).

39. Babiczky, A. & Matyas, F. Molecular characteristics and laminar distribution of prefrontal neurons projecting to the mesolimbic system. *Elife* **11** (2022).

40. Kast, R.J., Lanjewar, A.L., Smith, C.D. & Levitt, P. FOXP2 exhibits projection neuron class specific expression, but is not required for multiple aspects of cortical histogenesis. *Elife* **8** (2019).

41. Yao, Z.*, et al.* A transcriptomic and epigenomic cell atlas of the mouse primary motor cortex. *Nature* **598**, 103-110 (2021).

42. Hunskaar, S. & Hole, K. The formalin test in mice: dissociation between inflammatory and non-inflammatory pain. *Pain* **30**, 103-114 (1987).

43. Liu, J.*, et al.* Activation of Parvalbumin Neurons in the Rostro-Dorsal Sector of the Thalamic Reticular Nucleus Promotes Sensitivity to Pain in Mice. *Neuroscience* **366**, 113-123 (2017).
44. Poorthuis, R.B., Bloem, B., Schak, B., Wester, J., de Kock, C.P. & Mansvelder, H.D. Layer-specific modulation of the prefrontal cortex by nicotinic acetylcholine receptors. *Cereb Cortex* **23**, 148-161 (2013).
45. Guillem, K.*, et al.* Nicotinic acetylcholine receptor β2 subunits in the medial prefrontal cortex control attention. *Science* **333**, 888-891 (2011).
46. Bloem, B., Poorthuis, R.B. & Mansvelder, H.D. Cholinergic modulation of the medial prefrontal cortex: the role of nicotinic receptors in attention and regulation of neuronal activity. *Front Neural Circuits* **8**, 17 (2014).
47. Oswald, M.J.*, et al.* Cholinergic basal forebrain nucleus of Meynert regulates chronic pain-like behavior via modulation of the prelimbic cortex. *Nat Commun* **13**, 5014 (2022).
48. Radzicki, D., Pollema-Mays, S.L., Sanz-Clemente, A. & Martina, M. Loss of M1 Receptor Dependent Cholinergic Excitation Contributes to mPFC Deactivation in Neuropathic Pain. *J Neurosci* **37**, 2292-2304 (2017).
49. Peron, S.*, et al.* Recurrent interactions in local cortical circuits. *Nature* **579**, 256-259 (2020).
50. Le Merre, P., Ahrlund-Richter, S. & Carlen, M. The mouse prefrontal cortex: Unity in diversity. *Neuron* **109**, 1925-1944 (2021).
51. Smith, A.C.W.*, et al.* A master regulator of opioid reward in the ventral prefrontal cortex. *Science* **384**, eadn0886 (2024).
52. Sherman, S.M. Thalamus plays a central role in ongoing cortical functioning. *Nat Neurosci* **19**, 533-541 (2016).
53. Collins, D.P., Anastasiades, P.G., Marlin, J.J. & Carter, A.G. Reciprocal Circuits Linking the Prefrontal Cortex with Dorsal and Ventral Thalamic Nuclei. *Neuron* **98**, 366-379 e364 (2018).
54. De Ridder, D., Adhia, D. & Vanneste, S. The anatomy of pain and suffering in the brain and its clinical implications. *Neurosci Biobehav Rev* **130**, 125-146 (2021).
55. Naser, P.V. & Kuner, R. Molecular, Cellular and Circuit Basis of Cholinergic Modulation of Pain. *Neuroscience* **387**, 135-148 (2018).
56. Sullere, S., Kunczt, A. & McGehee, D.S. A cholinergic circuit that relieves pain despite opioid tolerance. *Neuron* **111**, 3414-3434 e3415 (2023).
57. Umana, I.C., Daniele, C.A. & McGehee, D.S. Neuronal nicotinic receptors as analgesic targets: it's a winding road. *Biochem Pharmacol* **86**, 1208-1214 (2013).
58. Nirogi, R., Goura, V., Abraham, R. & Jayarajan, P. alpha4beta2* neuronal nicotinic receptor ligands (agonist, partial agonist and positive allosteric modulators) as therapeutic prospects for pain. *Eur J Pharmacol* **712**, 22-29 (2013).
59. Mansvelder, H.D., Keath, J.R. & McGehee, D.S. Synaptic mechanisms underlie nicotine-induced excitability of brain reward areas. *Neuron* **33**, 905-919 (2002).
60. Bailey, C.D., Alves, N.C., Nashmi, R., De Biasi, M. & Lambe, E.K. Nicotinic α5 subunits drive developmental changes in the activation and morphology of prefrontal cortex layer VI neurons. *Biol Psychiatry* **71**, 120-128 (2012).
61. Ramirez-Latorre, J., Yu, C.R., Qu, X., Perin, F., Karlin, A. & Role, L. Functional contributions of alpha5 subunit to neuronal acetylcholine receptor channels. *Nature* **380**, 347-351 (1996).
62. Labrakakis, C. The Role of the Insular Cortex in Pain. *Int J Mol Sci* **24** (2023).
63. Liu, Y.*, et al.* A subset of dopamine receptor-expressing neurons in the nucleus accumbens controls feeding and energy homeostasis. *Nat Metab* **6**, 1616-1631 (2024).
64. Zhao, Z.D.*, et al.* A molecularly defined D1 medium spiny neuron subtype negatively regulates cocaine addiction.

Sci Adv **8**, eabn3552 (2022).

65. Corder, G., Ahanonu, B., Grewe, B.F., Wang, D., Schnitzer, M.J. & Scherrer, G. An amygdalar neural ensemble that encodes the unpleasantness of pain. *Science* **363**, 276-281 (2019).

66. Chaplan, S.R., Bach, F.W., Pogrel, J.W., Chung, J.M. & Yaksh, T.L. Quantitative assessment of tactile allodynia in the rat paw. *J Neurosci Methods* **53**, 55-63 (1994).

980 **Figure legends**

981

982 **Figure 1. *Foxp2* specifically marks the outputs of mPFC to thalamus**

983 **a**, Diagram of the injections of CTB into the thalamus of wildtype mice (left). Representative
984 images of the mPFC in mice with CTB injected into the thalamic area (middle, left); the enlarged
985 images of the indicated regions (middle, top); the injection site of CTB (middle, bottom).
986 Percentage of the *Foxp2*$^+$ or *Foxp2*$^-$ cells of all CTB$^+$ neurons (top right); Percentage of the CTB$^+$
987 or CTB$^-$ cells of all *Foxp2*$^+$ neurons (bottom right). Scale bars: middle left, 200 μm; middle top, 20
988 μm; middle bottom, 500 μm. **b**, Same as **a** with CTB injected into the PAG. Scale bars: middle left,
989 200 μm; middle top, 20 μm; middle bottom, 500 μm. **c**, Representative image of the smFISH for
990 *Foxp2* (red), *Slc17a7* (green) and *Gad1* (white) in the mPFC (left) and the enlarged image of the
991 indicated region (top right), as well as the percentages of the *Foxp2*$^+$ neurons co-expressing
992 *Slc17a7* or *Gad1* (bottom right). Scale bars: left, 200 μm; top right, 20 μm. **d**, Representative image
993 of smFISH for *Foxp2* (red), *Etv1* (white) and *Ctgf* (green) in the mPFC (left) and the percentages
994 of the *Foxp2*$^+$ neurons co-expressing *Etv1* or *Ctgf* (right). Scale bar, 200 μm. **e-g**, Representative
995 image of the smFISH for *Foxp2* (red) and *Oprk1* (green) (**e**), *Pou3f1* (green) (**f**), and *Tshz2* (green
996 (**g**) in the mPFC (left) and the enlarged image of the indicated region (top right), as well as the
997 percentages of the *Foxp2*-only and *Foxp2-Oprk1/Pou3f1/Tshz2* double positive cells in the mPFC
998 (bottom right). Scale bars: left, 200 μm; top right, 20 μm. **h**, Diagram of the axon labeling strategy
999 (left), and representative images showing the mGFP and mRuby signals in the thalamic subregions
1000 (middle and right). Enlarged images of the indicated regions in PTN, MD and VM are shown in
1001 the inserted boxes. Scale bars: 100 μm; inserted boxes, 10 μm. **i**, Quantification of the mean mRuby
1002 fluorescence intensity per area in different brain regions. **j**, Diagram of the projection pattern of
1003 mPFC L6 neurons.

1004 Data are represented as mean ± SEM. 3V, third ventricle; AD, anterodorsal thalamus; Amy,
1005 amygdala; CTB: cholera toxin subunit B; DLPAG, dorsal lateral periaqueductal grey; NAc,
1006 nucleus accumbens; Hb, habenula nucleus; HPC, hippocampus; LD, laterodorsal thalamus; LPAG,

1007 lateral periaqueductal grey; MD, mediodorsal thalamus; PAG: periaqueductal gray; PTN,
1008 parataenial thalamic nucleus; PVT, paraventricular thalamus; Re, reuniens nucleus; Str, striatum;
1009 VM, ventromedial thalamus.
1010

1011 **Figure 2. The mPFC *Foxp2*$^{+}$ neurons are deactivated in response to acute and chronic pain**
1012 **a**, Diagram of the *in vivo* miniscopic calcium imaging (left) and a representative image of virus
1013 expression and GRIN lens implantation (right), Scale bar: 200 μm. **b**, An example field of view
1014 (left) and identified contours of neuronal regions of interest (right). **c**, Timeline of treatments and
1015 calcium recordings. **d**, Diagram of calcium recording for noxious heat stimulation. **e**, Left, heatmap
1016 of the calcium event frequency averaged to 1 min of bin of all neurons in response to and after the
1017 tail pinch stimulation (n = 270). The white dotted lines indicate the start and end of tail pinch,
1018 respectively. Right, representative traces showed fluorescence intensity changes (ΔF/F) from the
1019 identified individual neurons in response to and after the tail pinch stimulation. The red and the
1020 blue background indicate the time of during and after the tail pinch stimulation, respectively. **f**,
1021 Cumulative distribution of calcium event frequencies of baseline (BL) and during the tail pinch
1022 stimulation (left). Percentages of neurons that show no change (grey), decrease (red), and
1023 increase (yellow) in frequency in response to noxious heat during the last minute compared to
1024 the baseline (right). n = 248. **g**, Average calcium event frequencies of all identified neurons in
1025 baseline and during the last minute of heating. n = 248. **h-k**, Same as **d-g** but for formalin
1026 treatment. n = 302. **l**, Diagram of calcium recording before and after CFA injection. **m**, Averaged
1027 frequency of spontaneous calcium events of all the identified neurons in the baseline (n = 297),
1028 day 1 (n = 297) and day 7 (n = 344) after CFA injection. **n**, Heatmap of the calcium transient
1029 frequency averaged to 3 min of bin of the registered same neurons across different days (n = 124).
1030 **o**, Representative calcium traces of the same individual neurons that show decrease (red), no
1031 change (black), and increase (yellow) in the frequency in the baseline, day 1 and day 7 after CFA
1032 injection. **p**, Cumulative distribution of the calcium event frequency of the registered same neurons
1033 in baseline, day 1 and day 7 after CFA injection. **q**, Comparison of baseline and day 1 events (left);

the percentages of the neurons that show no change (grey), decrease (red), and increase (yellow) in frequency in 1 day after CFA injection (right). **r**, Same as **q** except it is for comparison of day 7 after CFA injection.

Data are represented as mean ± SEM. *p < 0.05, **p < 0.01, ***p < 0.001. Each dot indicates one individual neuron.

Figure 3. The mPFC *Foxp2*$^+$ neurons regulate both sensory and affective aspects of pain

a, Diagram of virus injection (left) and a representative image of TeNT-EYFP expression in the PL mPFC of *Foxp2*-Cre mice (right). Scale bar: 100 μm. **b**, Diagram of the von Frey test (VFT) (left). Paw withdrawal threshold of the mice assessed in VFT (right). **c**, Diagram of the hot plate test (HPT) (left). Paw withdrawal latency of the mice assessed in HPT (right). **d**, Diagram of the virus injection into the PL mPFC of the *Foxp2*-Cre mice (left) and a representative image of hM3Dq-mCherry expression in the mPFC (right). Scale bar: 100 μm. **e**, Paw withdrawal threshold (left) and latency (right) of the mice with mCherry or hM3Dq-mCherry expression assessed in VFT and HPT, respectively. **f**, Diagram of formalin test (left). Licking duration of the mice in response to formalin injection after CNO treatment and summarized licking duration in the phase 1 and phase 2 (right 3 panels). **g**, Diagram of CFA injection (left) and paw withdrawal threshold/latency assessed by VFT on post CFA day 2 (middle) and HPT on post CFA day 3 (right). **h**, Diagram of the conditioned place preference (CPP) test starting from post CFA day 5 (left). The time that mice spent in the chamber before and after the conditioning (middle) and CPP scores (right) of the mice in CPP test. The CPP score is calculated by subtracting the time that the mice spent in chamber coupled with CNO treatment in the pre-test from the one in the post-test.

Data are represented as mean ± SEM. Each dot indicated one mouse. *p < 0.05, **p < 0.01, ***p < 0.001; ns, no significant difference.

Figure 4. Projection-specific effects of the mPFC *Foxp2*$^+$ neurons on acute nociception

a, Diagram of virus injection and optical fiber implantation in the *Foxp2*-Cre mice (left).

1061 Representative images showing the injection site in PL mPFC (middle) and the cannula
1062 implantation above the projection to PTN (right). Scale bars: 100 μm. **b-c**, Diagram of surgery in
1063 the *Foxp2*-Cre mice (left) and representative images (right) showing the implantation of the optical
1064 fiber above the projection to MD (**b**) or VM (**c**). Scale bars: 100 μm. **d**, Paw withdrawal
1065 threshold/latency assessed by VFT (left) and HPT (right) of the GFP-expressing and ChR2-
1066 expressing mice with (on) or without (off) light stimulation targeting the projection to PTN. **e**, **f**,
1067 Same as the **d** but targeting the projection to MD (**e**) or VM (**f**). **g**, Diagram of formalin injection
1068 (left). Licking duration of the mice in response to formalin injection with light stimulation (second
1069 panel), and summarized licking duration in phase 1 and phase 2 (right two panels) targeting the
1070 projection to PTN. **h**, **i**, Same as **g** but targeting the projection to MD (**h**) or VM (**i**).
1071 Data are represented as mean ± SEM. Each dot in bar graph indicated one mouse. *p < 0.05, ***p
1072 < 0.001; ns, no significant difference.
1073

1074 **Figure 5. Projection-specific effects of the mPFC *Foxp2*$^{+}$ neurons on chronic inflammatory**
1075 **pain**
1076 **a**, Schematic diagram of the behavioral tests. **b**, Paw withdrawal threshold/latency assessed by
1077 VFT (left) and HPT (right) of the EYFP- or ChR2-expressing mice with (On) or without (Off) light
1078 stimulation targeting the projection to PTN. **c**, **d**, Same as **b** but targeting the projection to MD (**c**)
1079 or VM (**d**). **e**, The time spent in the chamber paired with light stimulation (left) and the CPP scores
1080 (right) of the mice targeting the projection to PTN. **f**, **g**, Same as **e** but targeting the projection to
1081 MD (**f**) or VM (**g**).
1082 Data are represented as mean ± SEM. Each dot indicated one mouse. *p < 0.05, **p < 0.01, ***p
1083 < 0.001; ns, no significant difference.
1084

1085 **Figure 6. The mPFC *Foxp2*$^{+}$ neurons receive cholinergic innervation from HDB which is**
1086 **antinociceptive**
1087 **a**, Monosynaptic retrograde rabies tracing of the PL mPFC *Foxp2*$^{+}$ neurons. The timeline and

1088 diagram of virus injection (left). Representative image showing the virus expression in the
1089 injection site and magnified image of the indicated region (right). Scale bars: 200 μm; inserted box,
1090 20 μm. **b**, Representative images showing the RV-EGFP labeled cells from the anterior to posterior
1091 HDB (left), and quantification of the labeled cells in HDB (right) along the Anterior-Posterior axis.
1092 Scale bars: 200 μm. **c**, Immunostaining of ChAT in HDB showing colocalization with RV-EGFP
1093 labeling (left) and an enlarged image of the indicated region (middle). Quantification of the $ChAT^+$
1094 cells among the GFP^+ cells (right). Scale bars: left, 200 μm; right, 20 μm. **d**, Diagram of the surgery
1095 of *ChAT*-Cre mice (left), and representative images showing the expression of the virus in HDB
1096 and fiber implantation in the PL mPFC (middle) as well as a magnified image of the indicated
1097 region (right). Scale bars, middle, 200 μm; right, 20 μm. **e**, Paw withdrawal threshold (left) and
1098 latency (right) of the mice expressing EYFP or ChR2 with (on) or without (off) light stimulation
1099 assessed in VFT and HPT, respectively. **f**, Diagram of CFA injection to induce chronic pain (left),
1100 and the paw withdrawal threshold (middle) and latency (right) of the mice with (on) or without
1101 (off) light stimulation after CFA treatment.
1102 Data are represented as mean ± SEM. Each dot indicated one mouse. *$p < 0.05$, **$p < 0.01$, ***p
1103 < 0.001; ns, no significant difference.
1104

1105 **Figure 7. Cell-type specific expression pattern of acetylcholine receptors in mPFC, and the**
1106 **α4β2 nAChR relieves pain through the *Foxp2*$^+$ neurons in mPFC**
1107 **a**, Left: smFISH for *Foxp2* (red), *Chrna4* (green) and *Chrna7* (white) in the mPFC and the enlarged
1108 image of the indicated region. Right: quantification of *Chrna4*$^+$ and *Chrna7*$^+$ cells among the
1109 *Foxp2*$^+$ cells. Scale bars: 200 μm; inserted box, 20 μm. **b**, Same as **a** but for *Oprk1* (green), *Chrna4*
1110 (red) and *Chrna7* (white). **c**, Same as **a** but for *Foxp2* (red) and *Chrm1* (green). **d**, Same as **a** but
1111 for *Foxp2* (red) and *Chrm2* (green). **e**, Percentages of the *Foxp2*$^+$ cells (left) and the *Oprk1*$^+$ cells
1112 (right) among the cells expressing different types of acetylcholine receptor. **f**, Summary of the
1113 expression pattern of acetylcholine receptors in the mPFC. **g**, Diagram (left) and validation (right)
1114 of the cannula implantation into the PL mPFC. Scale bar: 200 μm. **h**, Paw withdrawal threshold

1115 (left) and latency (right) of the mice assessed in VFT and HPT before and after the intracranial
1116 injection of ABT-594 (5 pmol/site) into the mPFC. **i**, Diagram of CFA injection (left) and paw
1117 withdrawal threshold (middle) and latency (right) of the mice assessed in VFT and HPT in response
1118 to intracranial injection of ABT-594. **j**, Diagram (left) and validation (right) of the virus injection
1119 and cannula implantation. Scale bar: 200 μm. **k**, Paw withdrawal threshold in VFT (left) and
1120 latency in HPT (right) of the mice in response to ABT-594 treatment and CNO treatment.
1121 Data are represented as mean ± SEM. Each dot indicated one mouse. *$p < 0.05$, **$p < 0.01$, ***p
1122 < 0.001; ns, no significant difference.
1123

1124 **Figure 8. Graphic summary of the HDB^{ChAT}→mPFC^{Foxp2}→thalamus connections in**
1125 **regulating different aspects of pain**

1126 In the mPFC, the major outputs to thalamus originate from the corticothalamic neurons, which are
1127 specifically marked by the expression of *Foxp2*. These neurons are drastically deactivated in
1128 response to various acute noxious stimulation and in chronic inflammatory pain, and activation of
1129 these neurons regulates different aspects of pain through segregated thalamic projections. The
1130 mPFC *Foxp2*$^{+}$ neurons project to PTN are involved in relieving both the sensory and affective
1131 aspects of pain, while the projection to MD relieves affective pain and the one to VM regulates
1132 coping behaviors, respectively. The mPFC *Foxp2*$^{+}$ neurons receive cholinergic innervation from
1133 the HDB and highly express the α4β2 nAChR, which relieves pain by activating the *Foxp2*$^{+}$
1134 neurons in mPFC.
1135

1136 **Extended data**

1137

1138 **Extended Data Fig. 1. *Foxp2* specifically marks the L6 corticothalamic neurons in the mPFC.**
1139 **a**, smFISH for *Ntsr1* (red) in the mPFC. Scale bar: 200 μm. **b**, UMAP showing the results of an
1140 integrated analysis of single-cell RNA sequencing and spatial transcriptomics with neuron types
1141 and layer information (left). Predicted expression patterns of *Foxp2* (middle left) and *Oprk1*
1142 (middle right). L, layer; CT, corticothalamic neurons; ET, extratelencephalic neurons; IT,
1143 intratelencephalic neurons; NP, near-projecting neurons. Predicted expression levels of *Foxp2* and
1144 *Oprk1* in the mPFC neuronal subtypes with layer information (right). **c**, Diagram of the injections
1145 of CTB into the contralateral mPFC (cPFC) of wildtype mice (left). Representative images of the
1146 mPFC in mice with CTB injected into cPFC (middle, left); the enlarged images of the indicated
1147 regions (middle, top); injection site of the CTB (middle, bottom). Percentage of the *Foxp2*$^+$ or
1148 *Foxp2*$^-$ cells of all CTB$^+$ neurons (top right); Percentage of the CTB$^+$ or CTB$^-$ cells of all *Foxp2*$^+$
1149 neurons (bottom right). Scale bars: middle left, 200 μm; middle top, 20 μm; middle bottom, 500
1150 μm. **d**, **e**, Same as **c** but for CTB injected into the amygdala (**d**) or NAc (**e**). **f**, Representative image
1151 showing the virus expression in the mPFC of *Foxp2*-Cre mice as indicated in the Figure 1H. **g-m**,
1152 The mGFP and synaptophysin-fused mRuby signals labeling the axon puncta of the mPFC *Foxp2*$^+$
1153 neurons in the known targets of the mPFC, including striatum (**g**), NAc (**h**), amygdala (**i**), PAG (**j**),
1154 HPC (**k**), HY (**l**) and VTA (**m**).
1155 3V, third ventricle; AQ, cerebral aqueduct; BMA, basomedial amygdala; CeA, central amygdala;
1156 DG, dentate gyrus; Hip, hippocampus; HY, hypothalamus; IPN, interpeduncular nucleus; LV,
1157 lateral ventricle; MRN, midbrain reticular nucleus; NAc, nucleus accumbens; SNr, substantia nigra,
1158 reticular part; VTA, ventral tegmental area.

1159

1160 **Extended Data Fig. 2. Expression pattern of *Foxp2* in the mPFC along the anterior-posterior**
1161 **axis.**
1162 **a**, smFISH for *Foxp2* (red), *Etv1* (white) and *Ctgf* (green) in the mPFC at 2.3 mm anterior to the

1163 bregma (left) and the percentages of the *Foxp2*$^+$ neurons co-expressing *Etv1* or *Ctgf* (right). Scale
1164 bar, 200 μm. **b**, **c**, Same as **a** but for the mPFC region 2.1 mm (**b**) or 1.7 mm (**c**) anterior to the
1165 bregma. **d**, Quantification of the normalized fluorescence signals of *Etv1* (blue), *Foxp2* (red) and
1166 *Ctgf* (green) in the mPFC from the pia to the white matter at the indicated sections of mPFC along
1167 the anterior-posterior axis.
1168 Data are represented as mean ± SEM. Each dot indicated one mouse.
1169

1170 **Extended Data Fig. 3. *In vivo* miniscopic calcium imaging of the mPFC *Foxp2*$^+$ neurons.**
1171 **a**, Frequency of the calcium events of the identified neurons during baseline (BL) and during tail
1172 pinch stimulation. The numbers of the neurons with increased or decreased frequency are indicated.
1173 **b**, Amplitude of the calcium events of the identified neurons during BL and during tail pinch
1174 stimulation. Only the neurons that exhibited calcium events during both sessions were included (n
1175 = 34). **c**, Licking duration of the mice before and after formalin injection. **d**, Same as **a** but for the
1176 formalin stimulation comparing BL with phase 1 (left) or BL with phase 2 (right). **e**, Same as **b**
1177 but for the formalin stimulation comparing BL with phase 1 and phase 2. Only the neurons that
1178 exhibited calcium events during all sessions were included (n = 196). **f**, Representative field of
1179 view images of the mice during recording in baseline, 1 day and 7 days after CFA injection. Some
1180 neuronal contours in the same locations are identified in different days and longitudinally
1181 registered as the same individual neurons, which are labeled in the images
1182 Data are represented as mean ± SEM. Each dot indicates an individual neuron. ns, no significant
1183 difference.
1184

1185 **Extended Data Fig. 4. Effects of inactivating the mPFC *Foxp2*$^+$ neurons on pain-related**
1186 **behaviors.**
1187 **a**, Diagram of the virus injection (left) and a representative image of hM4Di-mCherry expression
1188 in the PL mPFC of *Foxp2*-Cre mice (right). Scale bar: 100 μm. **b**, Paw withdrawal threshold and
1189 latency of the mice assessed by VFT (left) and HPT (right). **c**, Diagram of formalin test (left).

Licking duration of the mice in response to formalin injection after CNO treatment and summarized licking duration in the phase 1 and phase 2 (right 3 panels). **d**, Diagram of the conditioned place avoidance (CPA) test (left). The time that mice (CFA treated) spent in the chamber paired with CNO treatment (middle) and CPA scores (right) of the mice in CPA test. **e**, Representative images of the cFos expression in the mPFC after CNO treatment in the mCherry-expressing, hM4Di-mCherry-expressing or hM3Dq-mCherry-expressing mice. Right: quantification of the $cFos^+$ cells in the mPFC L6. Scale bar: 100 μm.

Data are represented as mean ± SEM. Each dot indicated one mouse. *$p < 0.05$, **$p < 0.01$, ns, no significant difference.

Extended Data Fig. 5. Inputs of the mPFC *Foxp2*$^+$ neurons.

a, Monosynaptic retrograde rabies tracing of the PL mPFC *Foxp2*$^+$ neurons (top left) and whole brain mapping. Representative images of brain regions with RV-EGFP labeled cells, including IC (top, 2nd), TH (top, 3rd), Hip (top, 4th), BLA (bottom left), HY (bottom, 2nd), PAG (bottom, 3rd) and PBN (bottom, 4th). Scale bars: 200 μm. **b**, Quantification of the retrogradely labeled cells in different brain regions.

Data are represented as mean ± SEM. Each dot indicated one mouse. 3V, third ventricle. Aq, cerebral aqueduct; BLA, basolateral amygdala; BMA, basomedial amygdalar nucleus; CeA, central amygdalar nucleus; CP, caudoputamen; CLA, claustrum; DR, dorsal raphe nucleus; HDB, horizonal diagonal band of Broca; HY, hypothalamus; IC, insula cortex; LA, lateral amygdalar nucleus; LC, locus ceruleus; LH, lateral hypothalamic area; LPO, lateral preoptic area; MA, magnocellular nucleus; MD, mediodorsal thalamus; OT, olfactory tube; PAG, periaqueductal gray; PBN, parabrachial nucleus; Pir, piriform area; Re, nucleus of reuniens; scp, superioi cerebellar pedunles; SI, substantial insominata; TH, thalamus; vHip, ventral hippocampus; VM, ventromedial thalamus; ZI, zona incerta.

Extended Data Fig. 6. Cell type-specific expression patterns of acetylcholine receptor in the

1217 **mPFC.**

1218 **a**, Left, representative images of smFISH experiments in the mPFC for *Foxp2* (red), *Chrna4* (green)
1219 and *Chrnb2* (white). An enlarged image of the indicated region is inserted in the bottom left box.
1220 Right: Quantification of *Chrna4*$^+$*Chrnb2*$^+$*Foxp2*$^+$ cells among all the *Foxp2*$^+$ cells. Scale bars: 200
1221 μm; inserted box, 20 μm. **b**, Left: same as **a** but for *Oprk1* (green), *Chrna4* (red) and *Chrnb2*
1222 (white). Right: Quantification of *Chrna4*$^+$*Chrnb2*$^+$*Oprk1*$^+$ cells among all the *Oprk1*$^+$ cells. **c**, Left:
1223 smFISH of *Oprk1* (red) and *Chrm1* (green) in the mPFC. Right: quantification of the
1224 *Chrm1*$^+$*Oprk1*$^+$ cells among all the *Oprk1*$^+$ cells. Scale bars: 200 μm; inserted box, 20 μm. **d**, Same
1225 as **c** but for *Oprk1* (red) and *Chrm2* (green) in the mPFC.

1226

1227 **Extended Data Fig. 7. Effects of activating the α4β2 nAChR in the mPFC.**

1228 **a**, Dosage test of ABT-594. Paw withdrawal threshold of the mice assessed in VFT before and after
1229 the intracranial injection of ABT-594 (2.5 pmol/site) (left) or ABT-594 (25 pmol/site) (right) into
1230 the mPFC compared to ACSF treatment. **b**, Schematic diagram for CPP test paired with ACSF or
1231 ABT-594 treatment (left) and the time in the chamber paired with ABT-594 treatment before and
1232 after the conditioning (middle) as well as the CPP scores of the mice (right).
1233 Data are represented as mean ± SEM. Each dot indicated one mouse. *$p < 0.05$, **$p < 0.01$, ***p
1234 < 0.001; ns, no significant difference.

Figure 1

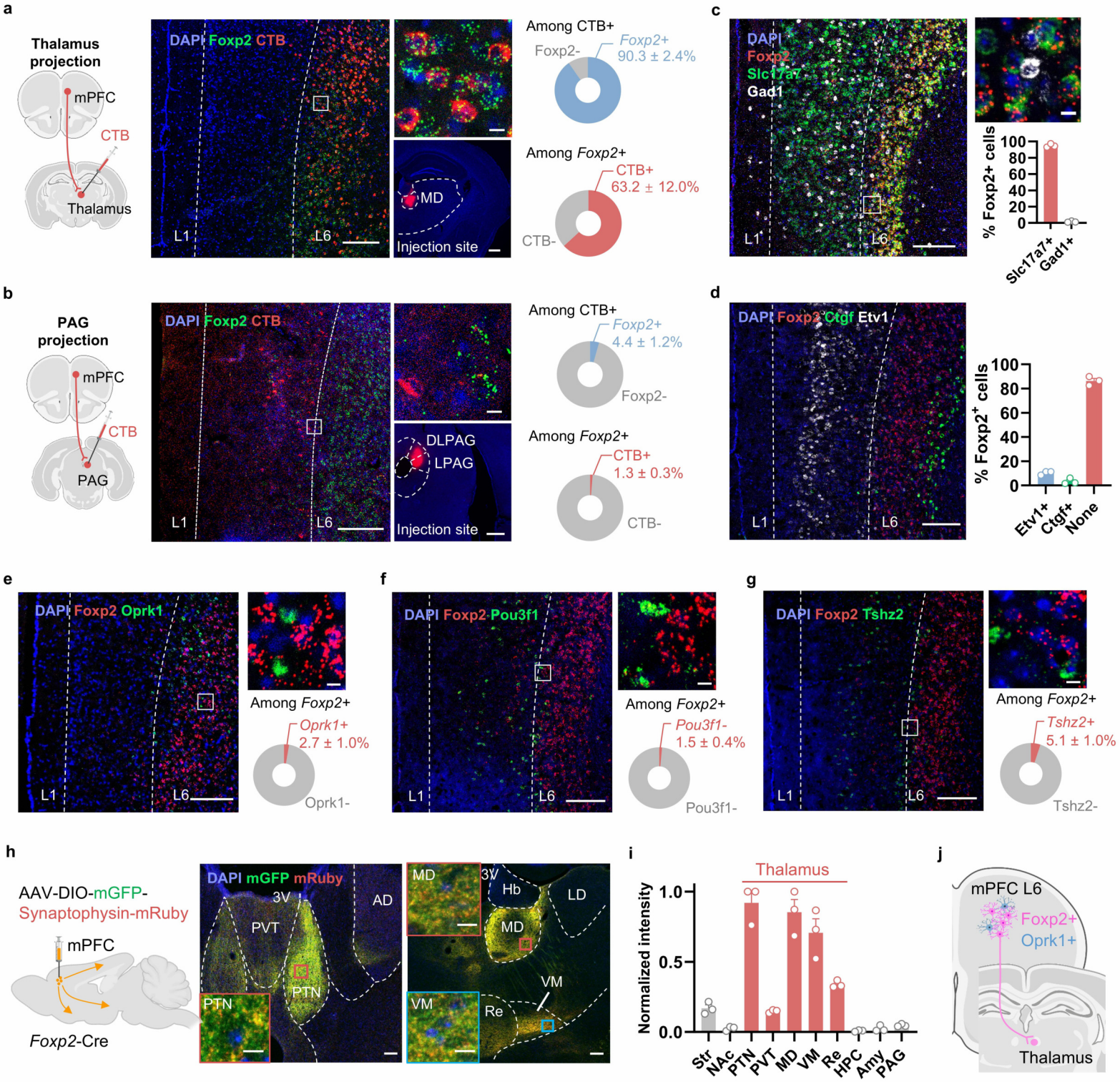
a
Thalamus projection
mPFC
CTB
Thalamus
DAPI Foxp2 CTB
L1
L6
MD
Injection site
Among CTB+
Foxp2-
Foxp2+
90.3 ± 2.4%
Among Foxp2+
CTB+
63.2 ± 12.0%
CTB-
b
PAG projection
mPFC
CTB
PAG
DAPI Foxp2 CTB
L1
L6
DLPAG
LPAG
Injection site
Among CTB+
Foxp2+
4.4 ± 1.2%
Foxp2-
Among Foxp2+
CTB+
1.3 ± 0.3%
CTB-
c
DAPI
Foxp2
Slc17a7
Gad1
L1
L6
% Foxp2+ cells
100
80
60
40
20
0
Slc17a7+
Gad1+
d
DAPI Foxp2 Ctgf Etv1
L1
L6
% Foxp2+ cells
100
80
60
40
20
0
Etv1+
Ctgf+
None
e
DAPI Foxp2 Oprk1
L1
L6
Among Foxp2+
Oprk1+
2.7 ± 1.0%
Oprk1-
f
DAPI Foxp2 Pou3f1
L1
L6
Among Foxp2+
Pou3f1-
1.5 ± 0.4%
Pou3f1-
g
DAPI Foxp2 Tshz2
L1
L6
Among Foxp2+
Tshz2+
5.1 ± 1.0%
Tshz2-
h
AAV-DIO-mGFP-
Synaptophysin-mRuby
mPFC
Foxp2-Cre
DAPI mGFP mRuby
3V
AD
PVT
PTN
PTN
MD
3V
Hb
LD
MD
VM
VM
Re
i
Thalamus
Normalized intensity
1.0
0.5
0.0
Str
NAc
PTN
PVT
MD
VM
Re
HPC
Amy
PAG
j
mPFC L6
Foxp2+
Oprk1+
Thalamus

Figure 2

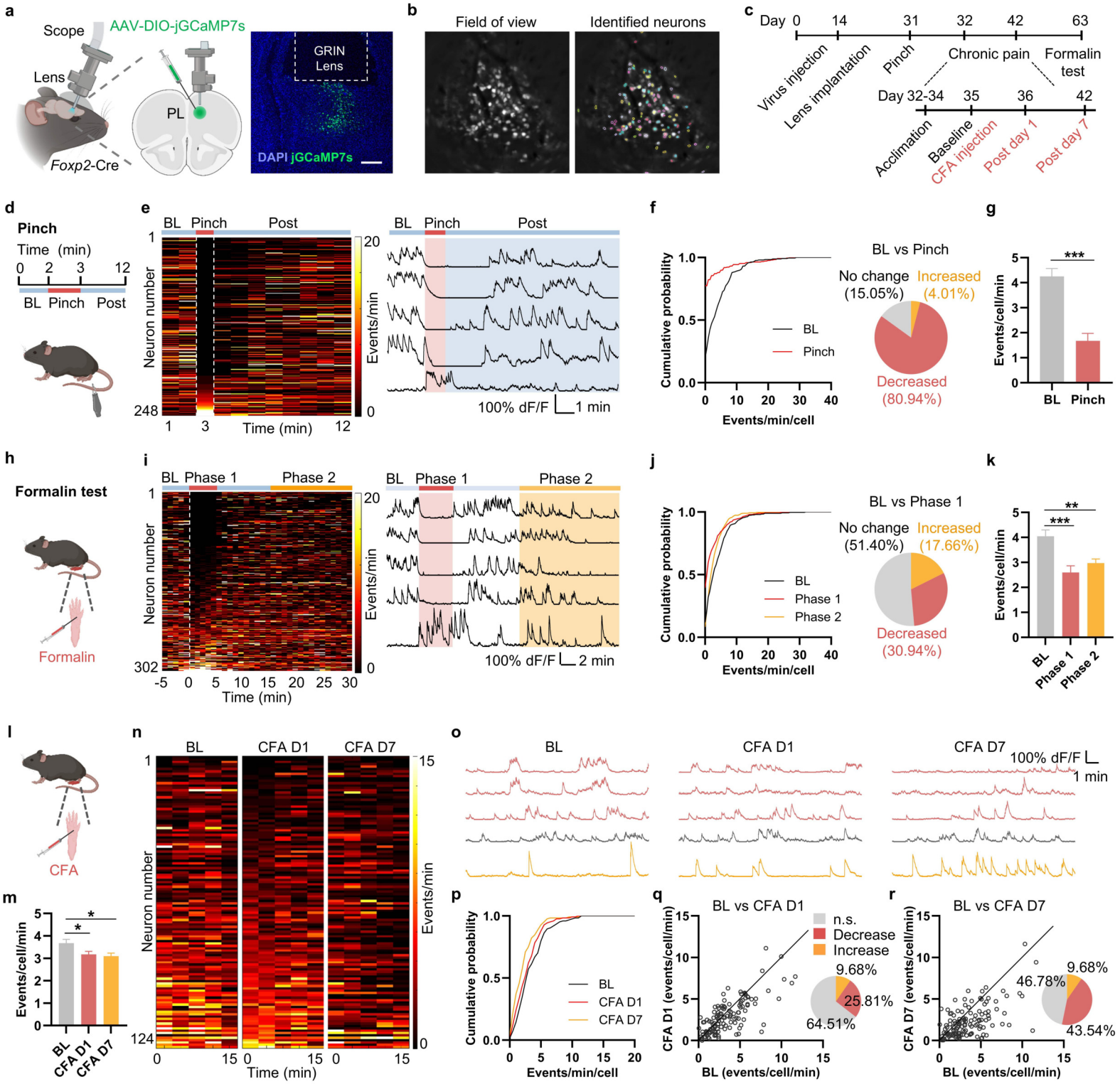
a
Scope
AAV-DIO-jGCaMP7s
Lens
PL
Foxp2-Cre
GRIN Lens
DAPI jGCaMP7s
b
Field of view
Identified neurons
c
Day 0 14 31 32 42 63
Virus injection
Lens implantation
Pinch
Chronic pain
Formalin test
Day 32-34 35 36 42
Acclimation
Baseline
CFA injection
Post day 1
Post day 7
d
Pinch
Time (min)
0 2 3 12
BL Pinch Post
e
BL Pinch Post
Neuron number
Events/min
Time (min)
100% dF/F
1 min
f
Cumulative probability
Events/min/cell
BL
Pinch
BL vs Pinch
No change (15.05%)
Increased (4.01%)
Decreased (80.94%)
g
Events/cell/min
***
BL Pinch
h
Formalin test
Formalin
i
BL Phase 1 Phase 2
Neuron number
Events/min
Time (min)
100% dF/F
2 min
j
Cumulative probability
Events/min/cell
BL
Phase 1
Phase 2
BL vs Phase 1
No change (51.40%)
Increased (17.66%)
Decreased (30.94%)
k
Events/cell/min
**
***
BL Phase 1 Phase 2
l
CFA
m
Events/cell/min
*
*
BL CFA D1 CFA D7
n
BL CFA D1 CFA D7
Neuron number
Events/min
Time (min)
o
BL CFA D1 CFA D7
100% dF/F
1 min
p
Cumulative probability
Events/min/cell
BL
CFA D1
CFA D7
q
BL vs CFA D1
n.s.
Decrease
Increase
9.68%
25.81%
64.51%
CFA D1 (events/cell/min)
BL (events/cell/min)
r
BL vs CFA D7
46.78%
9.68%
43.54%
CFA D7 (events/cell/min)
BL (events/cell/min)

Figure 3

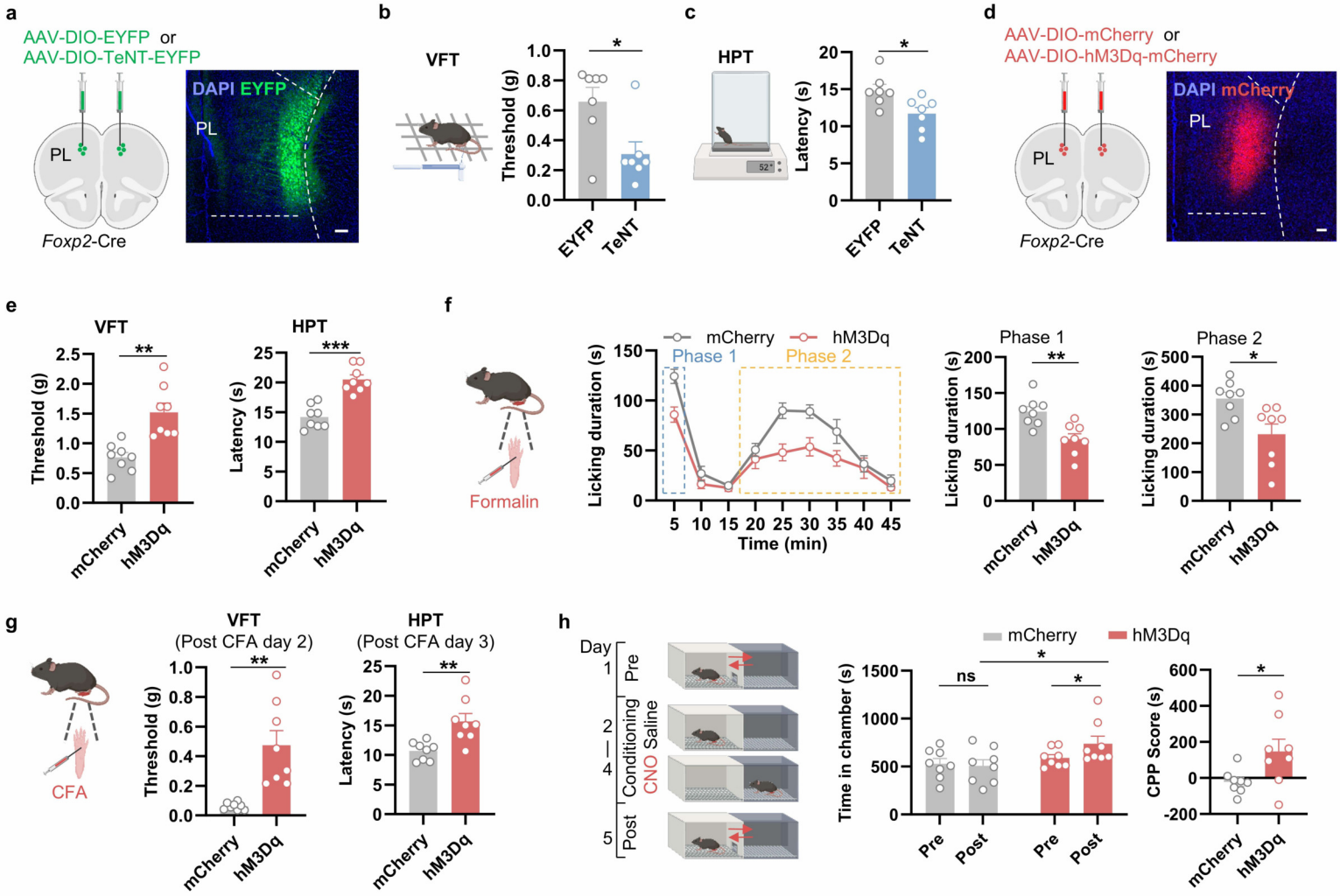
a
AAV-DIO-EYFP or
AAV-DIO-TeNT-EYFP
PL
Foxp2-Cre
DAPI EYFP
PL
b
VFT
Threshold (g)
EYFP
TeNT
c
HPT
Latency (s)
EYFP
TeNT
d
AAV-DIO-mCherry or
AAV-DIO-hM3Dq-mCherry
PL
Foxp2-Cre
DAPI mCherry
PL
e
VFT
Threshold (g)
mCherry
hM3Dq
HPT
Latency (s)
mCherry
hM3Dq
f
Formalin
mCherry
hM3Dq
Phase 1
Phase 2
Licking duration (s)
Time (min)
Phase 1
Licking duration (s)
mCherry
hM3Dq
Phase 2
Licking duration (s)
mCherry
hM3Dq
g
CFA
VFT
(Post CFA day 2)
Threshold (g)
mCherry
hM3Dq
HPT
(Post CFA day 3)
Latency (s)
mCherry
hM3Dq
h
Day
Pre
Conditioning
CNO Saline
Post
mCherry
hM3Dq
Time in chamber (s)
ns
Pre
Post
Pre
Post
CPP Score (s)
mCherry
hM3Dq

Figure 4

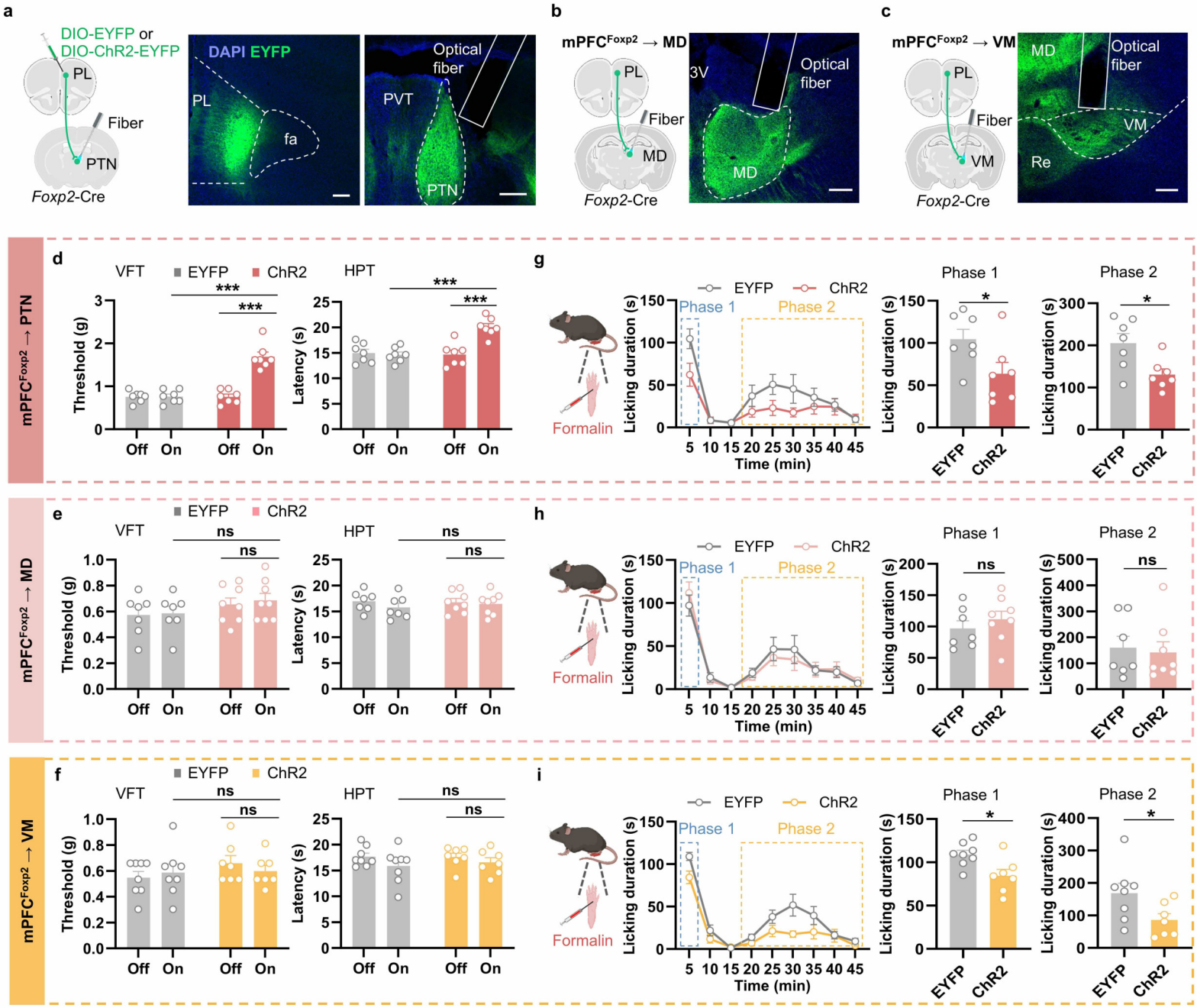
a
DIO-EYFP or
DIO-ChR2-EYFP
PL
Fiber
PTN
Foxp2-Cre
DAPI EYFP
PL
fa
Optical fiber
PVT
PTN
b
mPFCFoxp2 → MD
PL
Fiber
MD
Foxp2-Cre
3V
Optical fiber
MD
c
mPFCFoxp2 → VM
PL
Fiber
VM
Foxp2-Cre
MD
Optical fiber
VM
Re
mPFCFoxp2 → PTN
d
VFT
EYFP
ChR2
HPT
Threshold (g)
Latency (s)
Off
On
***
g
Formalin
Licking duration (s)
Phase 1
Phase 2
Time (min)
EYFP
ChR2
*
mPFCFoxp2 → MD
e
ns
h
mPFCFoxp2 → VM
f
i

Figure 5

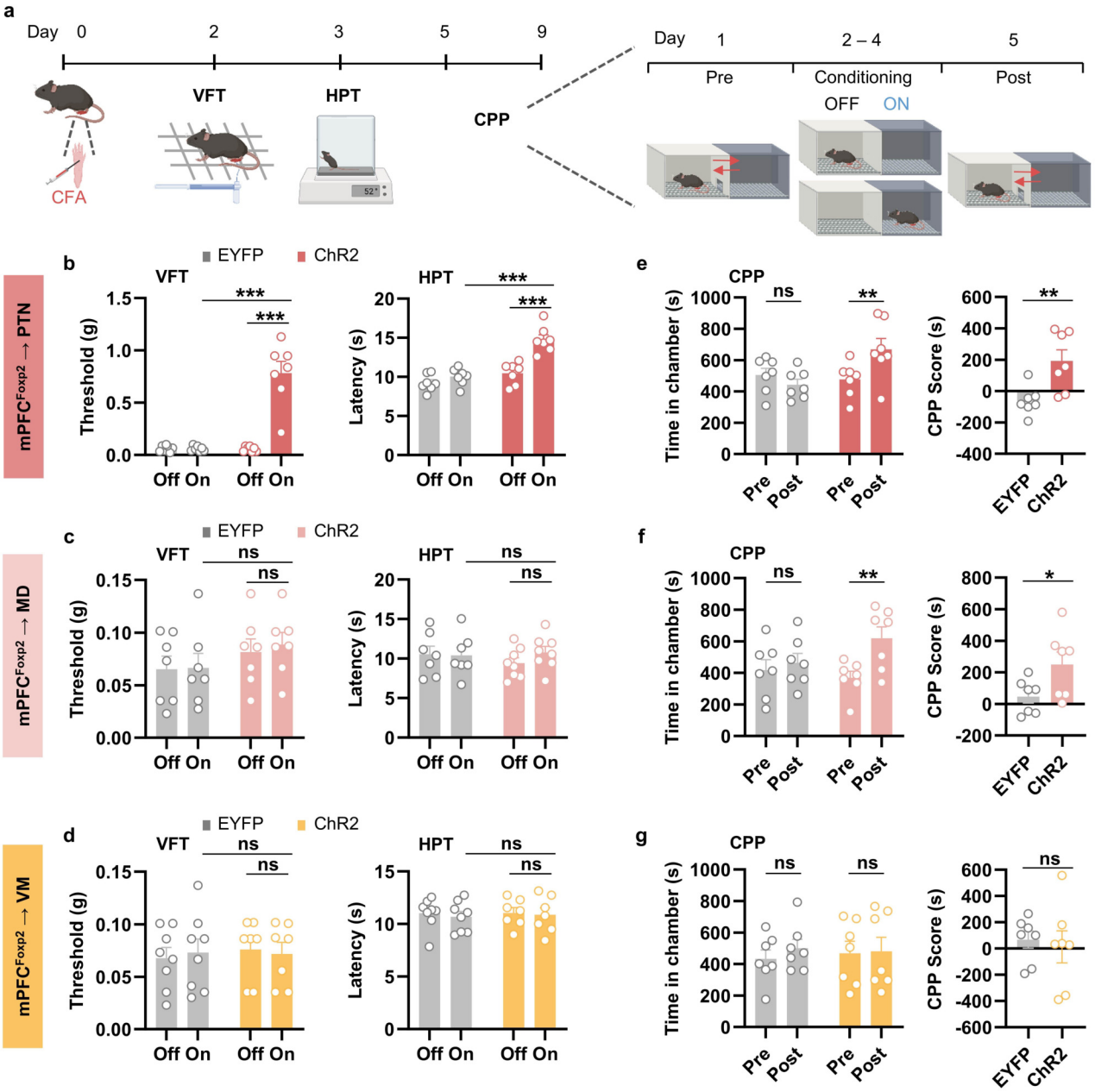
a
Day 0
2
3
5
9
CFA
VFT
HPT
CPP
Day 1
2 – 4
5
Pre
Conditioning
Post
OFF
ON
mPFC^Foxp2 → PTN
mPFC^Foxp2 → MD
mPFC^Foxp2 → VM
EYFP
ChR2
b
c
d
e
f
g
VFT
HPT
CPP
Threshold (g)
Latency (s)
Time in chamber (s)
CPP Score (s)
Off On
Pre
Post
EYFP
ChR2
***
**
*
ns

Figure 6

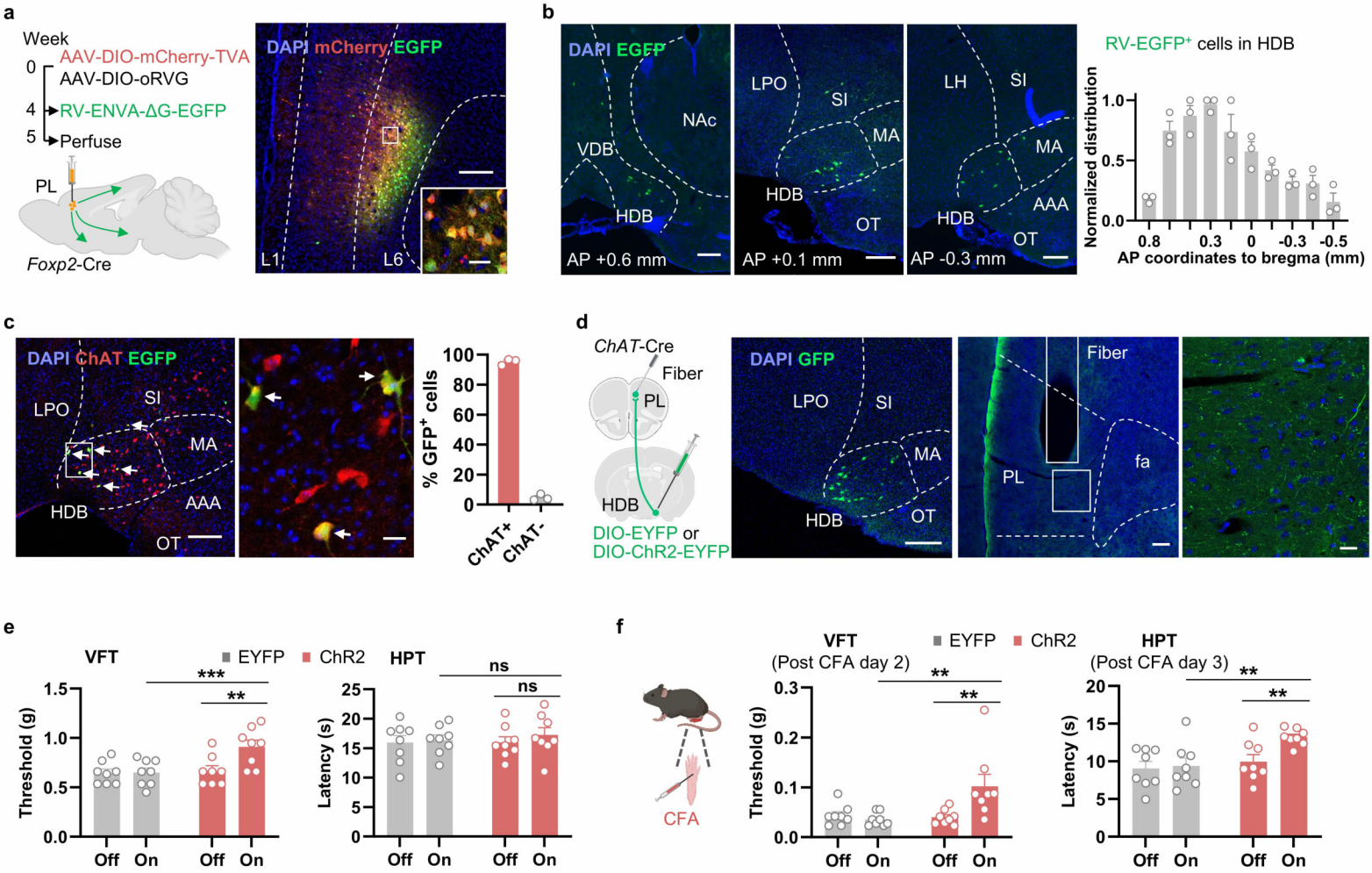
a
Week
0
AAV-DIO-mCherry-TVA
AAV-DIO-oRVG
4
RV-ENVA-ΔG-EGFP
5
Perfuse
PL
Foxp2-Cre
DAPI mCherry EGFP
L1
L6
b
DAPI EGFP
NAc
VDB
HDB
AP +0.6 mm
LPO
SI
MA
HDB
OT
AP +0.1 mm
LH
SI
MA
AAA
HDB
OT
AP -0.3 mm
RV-EGFP+ cells in HDB
Normalized distribution
1.0
0.5
0.0
0.8
0.3
0
-0.3
-0.5
AP coordinates to bregma (mm)
c
DAPI ChAT EGFP
LPO
SI
MA
HDB
AAA
OT
% GFP+ cells
100
80
60
40
20
0
ChAT+
ChAT-
d
ChAT-Cre
Fiber
PL
HDB
DIO-EYFP or
DIO-ChR2-EYFP
DAPI GFP
LPO
SI
MA
HDB
OT
Fiber
PL
fa
e
VFT
EYFP
ChR2
HPT
Threshold (g)
Latency (s)
***
**
ns
ns
Off
On
Off
On
f
CFA
VFT
(Post CFA day 2)
EYFP
ChR2
HPT
(Post CFA day 3)
Threshold (g)
Latency (s)
**
**
**
**
Off
On
Off
On

Figure 7

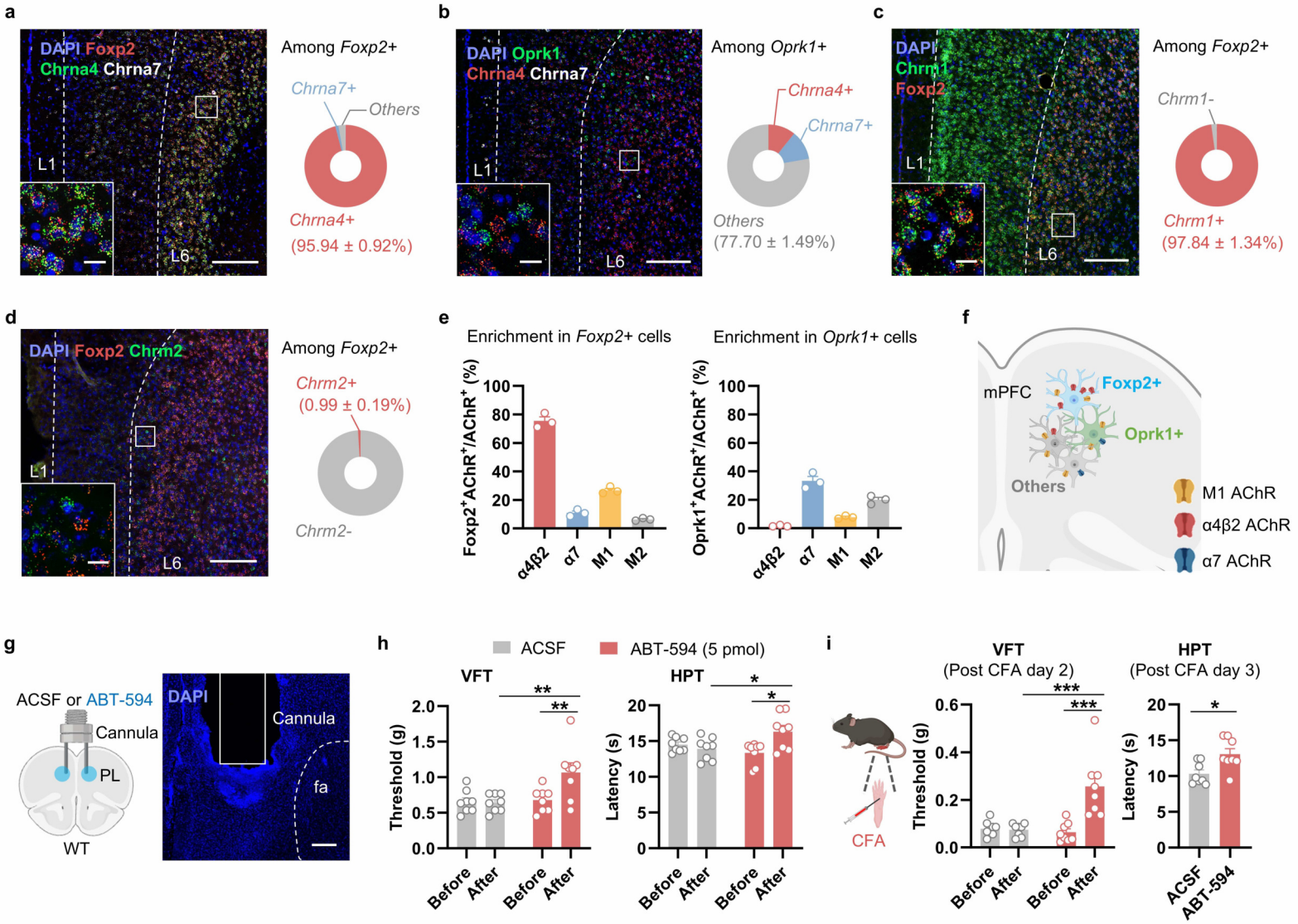
a
DAPI Foxp2
Chrna4 Chrna7
L1
L6
Among Foxp2+
Chrna7+
Others
Chrna4+
(95.94 ± 0.92%)
b
DAPI Oprk1
Chrna4 Chrna7
Among Oprk1+
Chrna4+
Chrna7+
Others
(77.70 ± 1.49%)
c
DAPI
Chrm1
Foxp2
Among Foxp2+
Chrm1-
Chrm1+
(97.84 ± 1.34%)
d
DAPI Foxp2 Chrm2
Among Foxp2+
Chrm2+
(0.99 ± 0.19%)
Chrm2-
e
Enrichment in Foxp2+ cells
Enrichment in Oprk1+ cells
Foxp2+AChR+/AChR+ (%)
Oprk1+AChR+/AChR+ (%)
α4β2
α7
M1
M2
f
mPFC
Foxp2+
Oprk1+
Others
M1 AChR
α4β2 AChR
α7 AChR
g
ACSF or ABT-594
Cannula
PL
WT
DAPI
Cannula
fa
h
ACSF
ABT-594 (5 pmol)
VFT
HPT
Threshold (g)
Latency (s)
Before
After
i
CFA
VFT
(Post CFA day 2)
HPT
(Post CFA day 3)
Threshold (g)
Latency (s)
ACSF
ABT-594
j
ACSF or ABT-594
AAV-DIO-
-hM4Di-mCherry
PL
i.p. CNO
Foxp2-Cre
DAPI
mCherry
Cannula
fa
k
VFT
HPT
Threshold (g)
ns
ACSF + Saline
ABT + Saline
ABT + CNO
mCherry
hM4Di

Figure 8

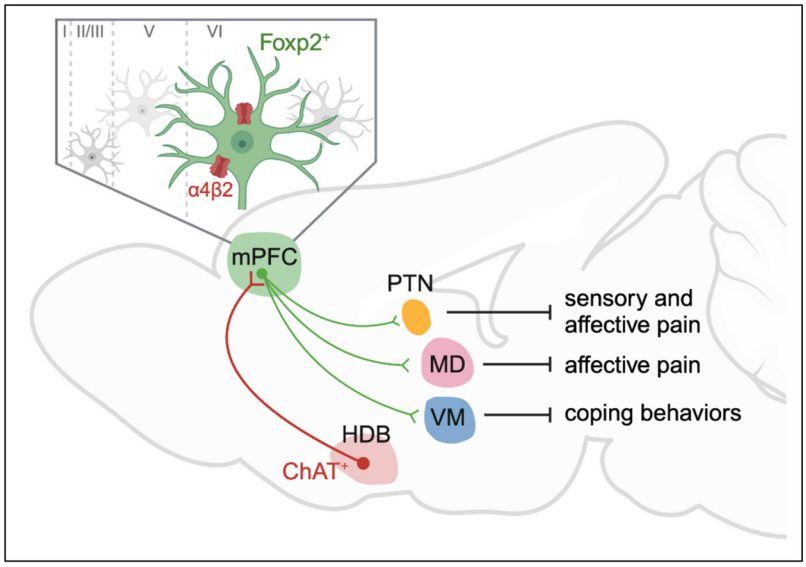
I-II/III
V
VI
Foxp2+
α4β2
mPFC
PTN
sensory and
affective pain
MD
affective pain
VM
coping behaviors
HDB
ChAT+

Extended Data Fig. 1

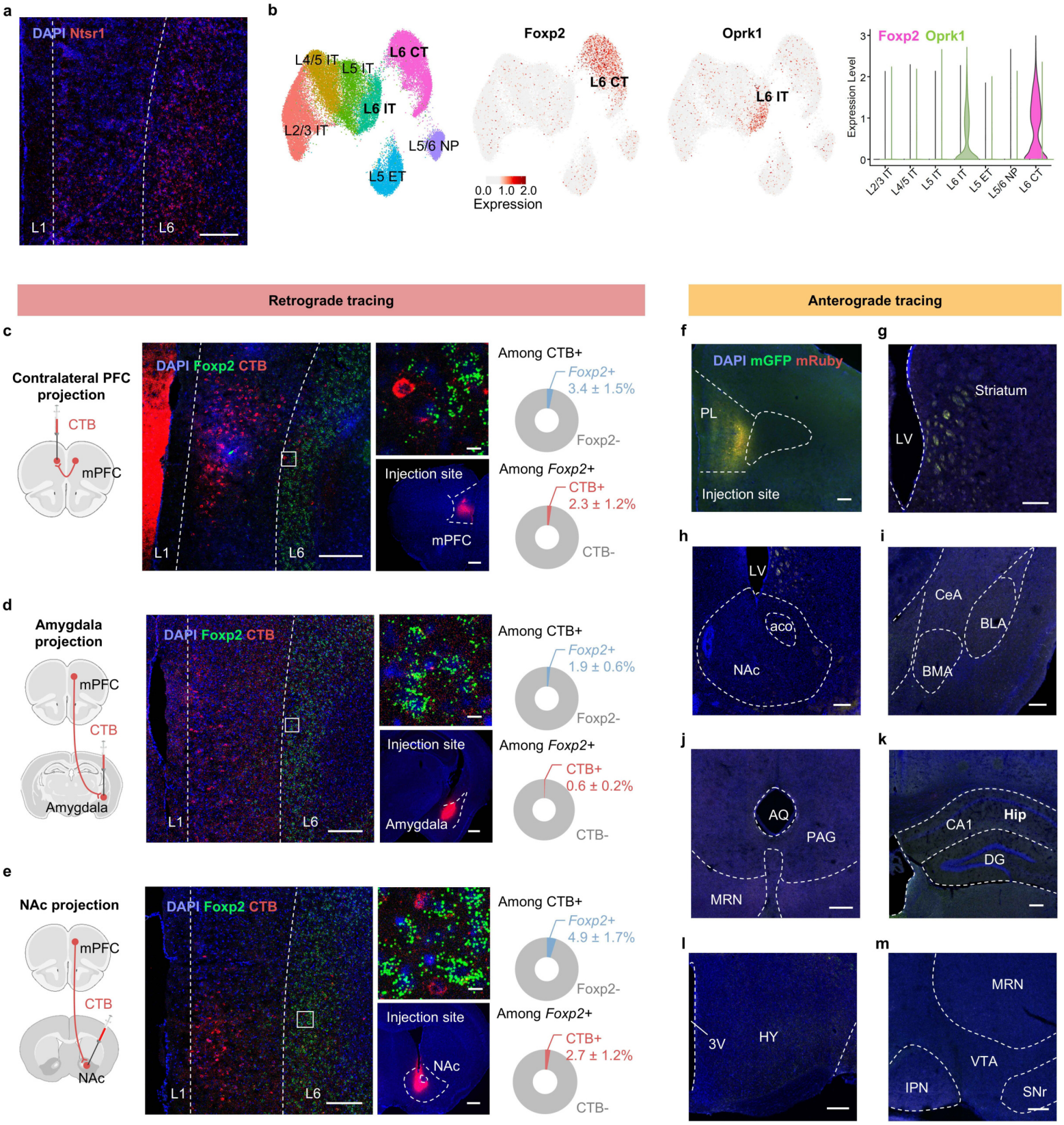

Extended Data Fig. 2

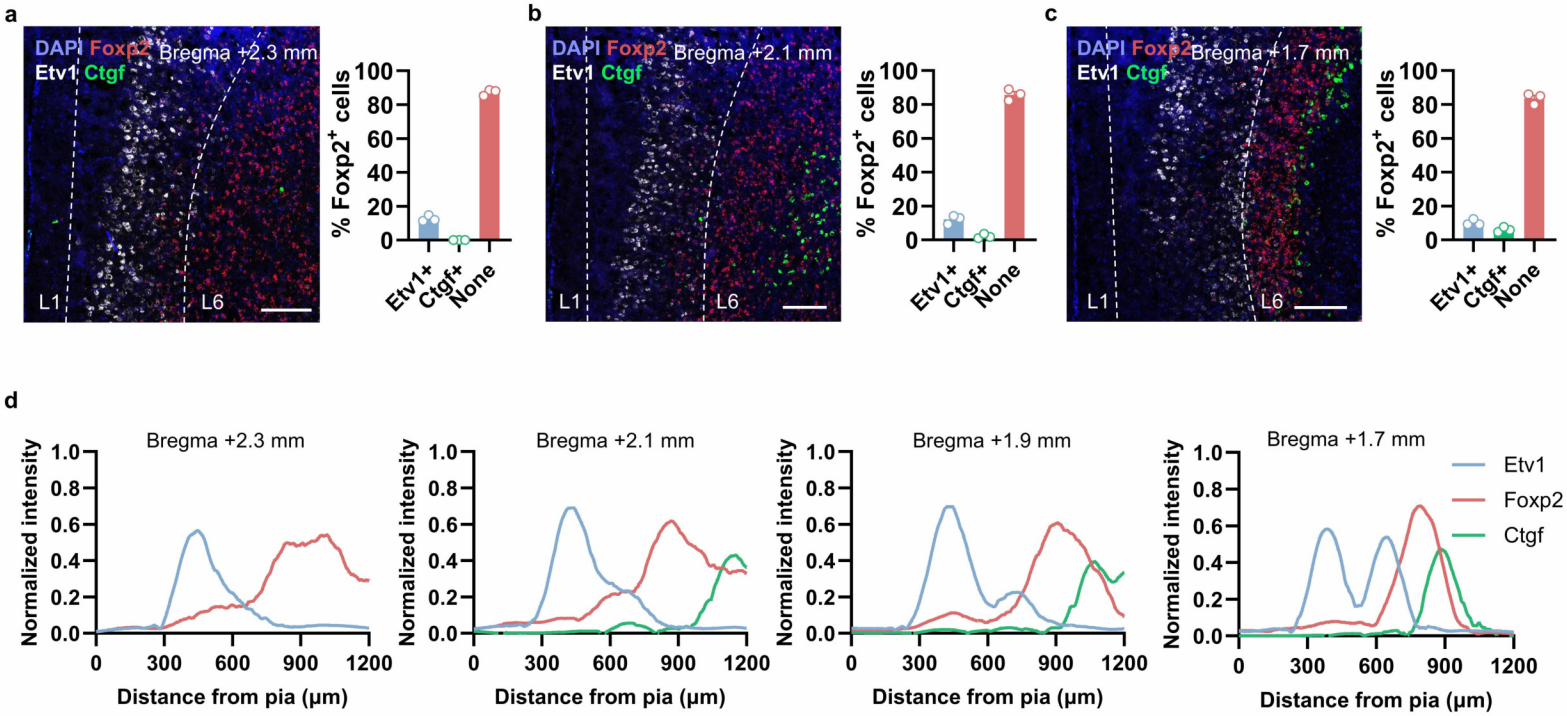

Extended Data Fig. 3

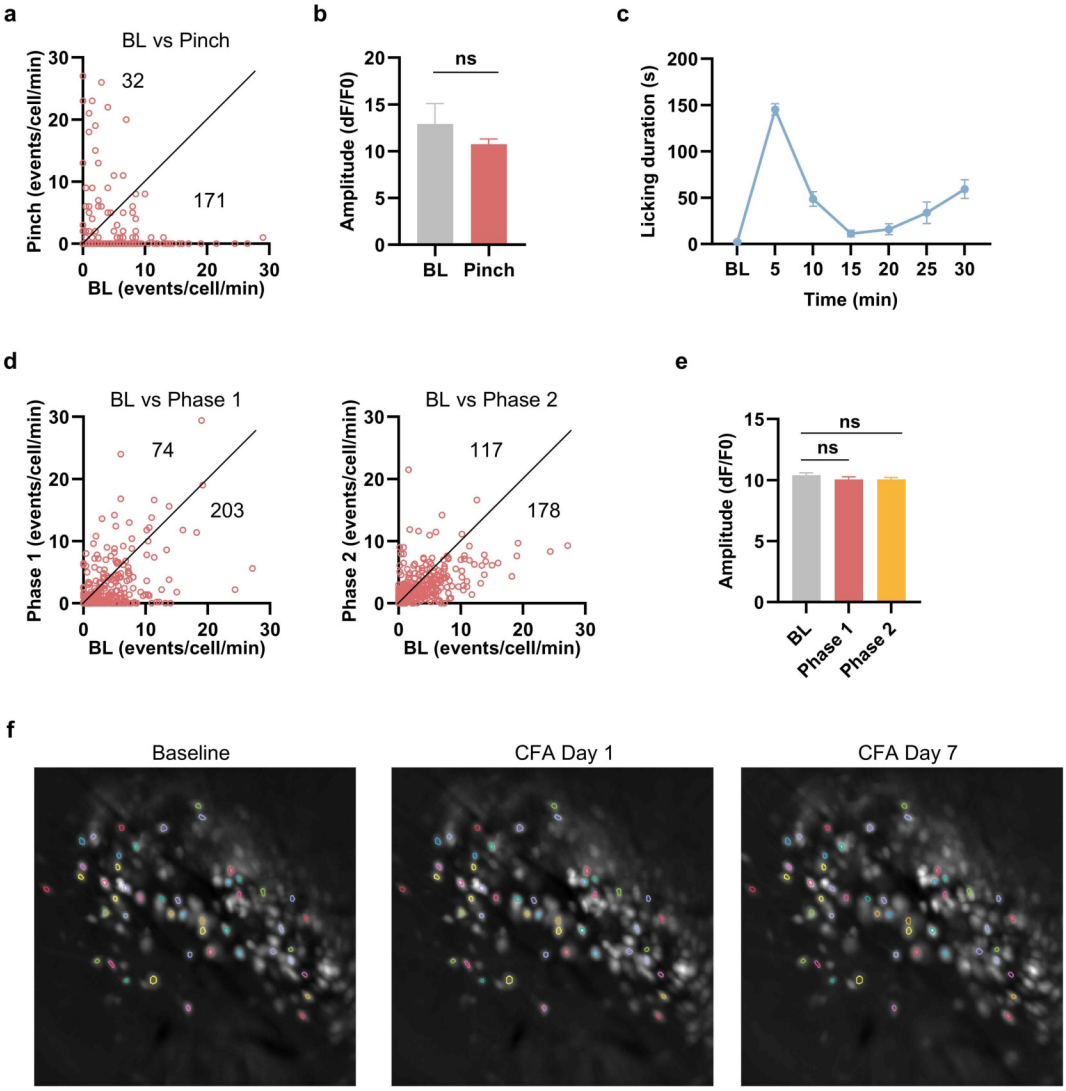

Extended Data Fig. 4

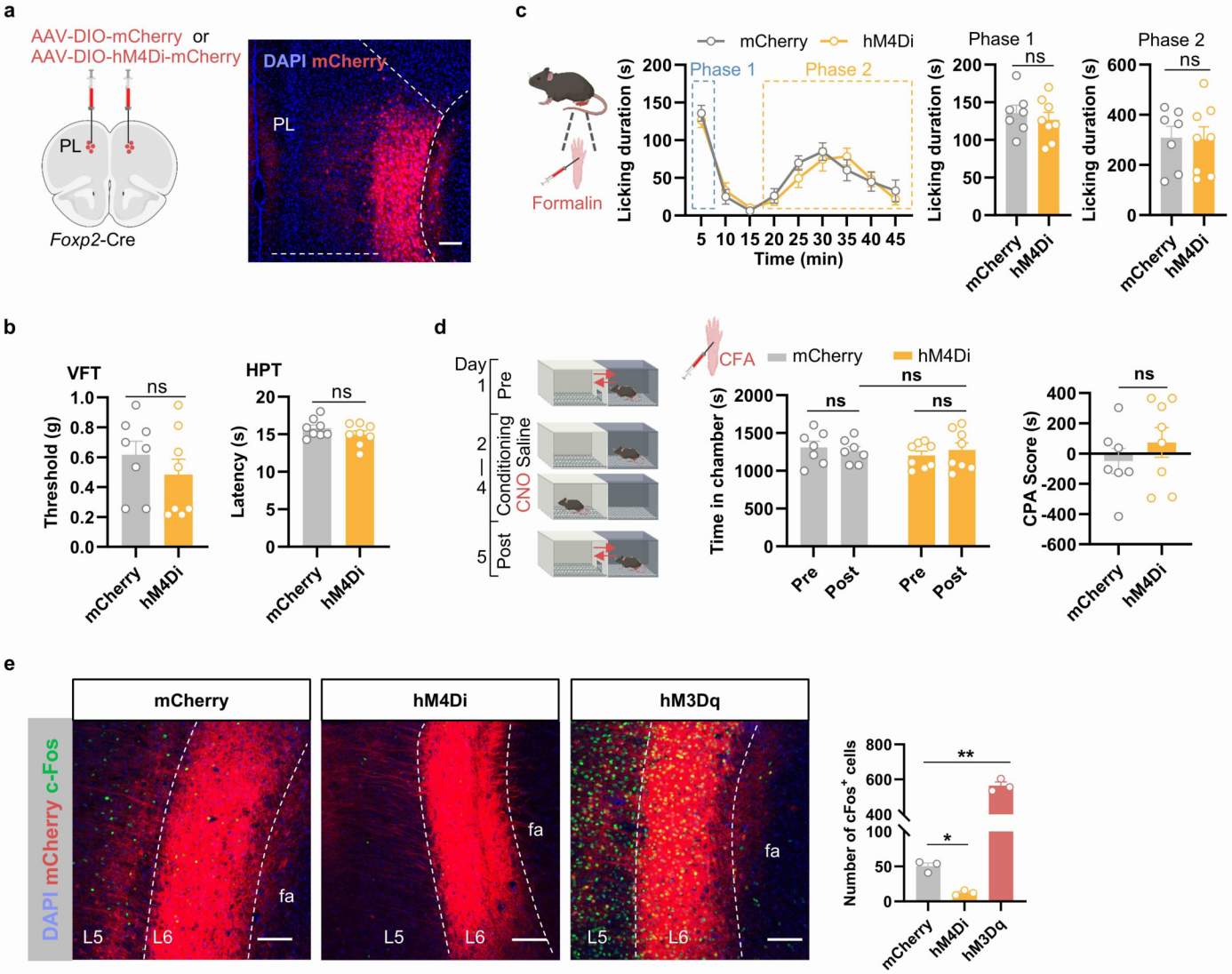

Extended Data Fig. 5

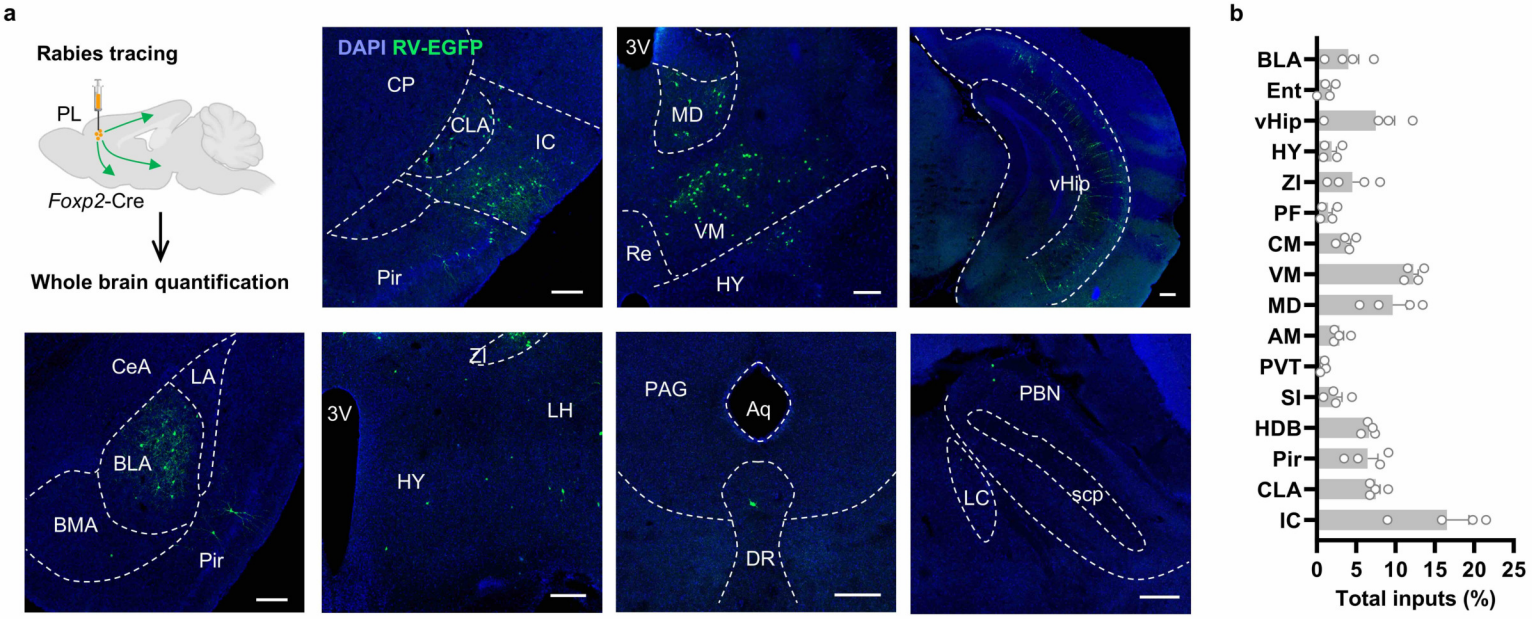

Extended Data Fig. 6

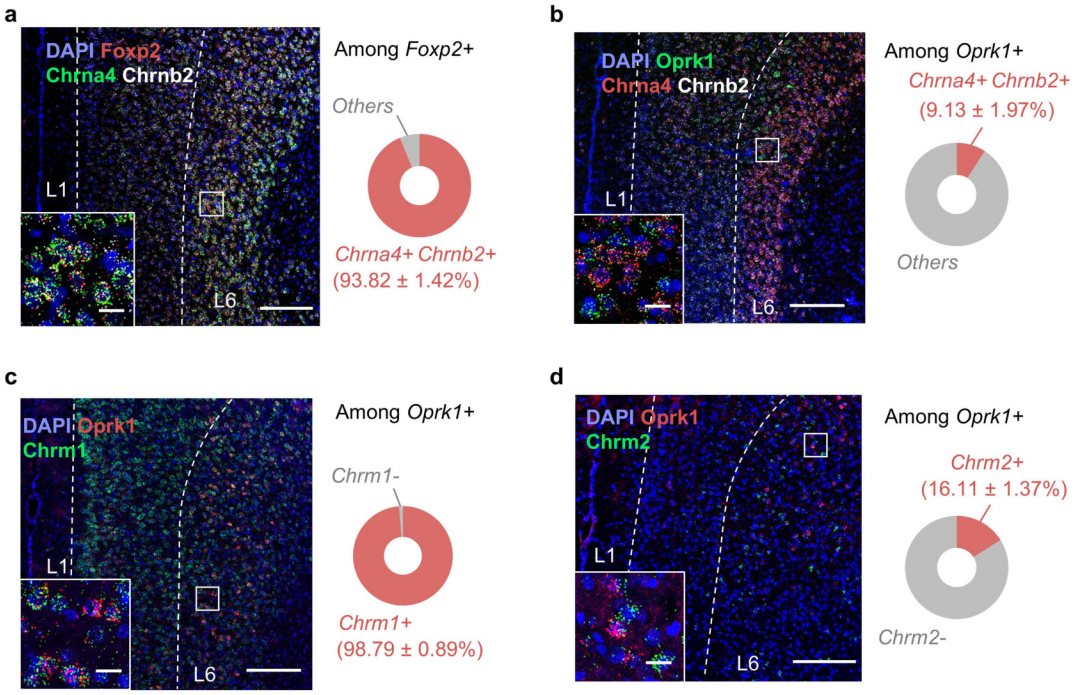
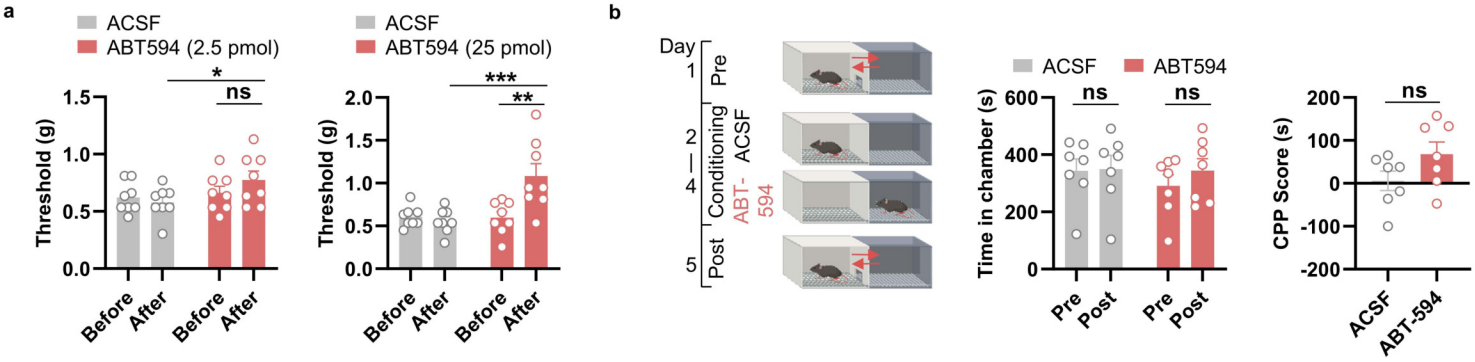
Extended Data Fig. 7